

RESEARCH

Open Access



# Tyrosine kinase inhibitor-loaded biomimetic nanoparticles as a treatment for osteosarcoma

Federica Giordano<sup>1,2†</sup>, Stefania Lenna<sup>1,2†</sup>, Gherardo Baudo<sup>1,2,5</sup>, Riccardo Rampado<sup>1,2,4</sup>, Matteo Massaro<sup>1,2,5</sup>, Enrica De Rosa<sup>1,2</sup>, April Ewing<sup>1,2</sup>, Lyazat Kurenbekova<sup>3</sup>, Marco Agostini<sup>4</sup>, Jason T. Yustein<sup>3\*</sup> and Francesca Taraballi<sup>1,2\*</sup>

<sup>†</sup>Federica Giordano and Stefania Lenna contributed equally to this work

\*Correspondence: yustein@bcm.edu; Ftaraballi2@houstonmethodist.org

<sup>1</sup>Center for Musculoskeletal Regeneration, Houston Methodist Research Institute, Houston, TX 77030, USA

<sup>2</sup>Orthopedics and Sports Medicine, Houston Methodist Hospital, Houston, TX 77030, USA

<sup>3</sup>Texas Children's Cancer and Hematology Center, The Faris D. Virani Ewing Sarcoma Center, Baylor College of Medicine, Houston, TX 77030, USA

<sup>4</sup>Nano-Inspired Biomedicine Laboratory, Institute of Pediatric Research—Città della Speranza, Padua, Italy

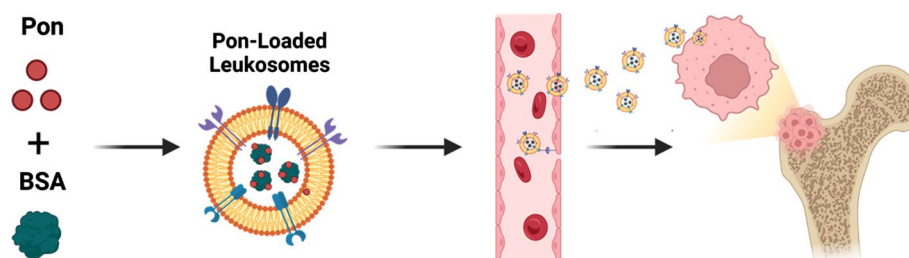
<sup>5</sup>College of Materials Sciences and Opto-Electronic Technology, University of Chinese Academy of Sciences, 100049 Beijing, China

## Abstract

Small-molecule tyrosine kinase inhibitors (TKIs) represent a potentially powerful approach to the treatment of osteosarcoma (OS). However, dose-limiting toxicity, therapeutic efficacy, and targeting specificity are significant barriers to the use of TKIs in the clinic. Notably among TKIs, ponatinib demonstrated potent anti-tumor activity; however, it received an FDA black box warning for potential side effects. We propose ponatinib-loaded biomimetic nanoparticles (NPs) to repurpose ponatinib as an efficient therapeutic option for OS. In this study, we demonstrate enhanced targeting ability and maintain potent ponatinib nano-therapeutic activity, while also reducing toxicity. In in vitro two- and three-dimensional models, we demonstrate that ponatinib-loaded biomimetic NPs maintain the efficacy of the free drug, while in vivo we show that they can improve tumor targeting, slow tumor growth, and reduce evidence of systemic toxicities. Though there is limited Pon encapsulation within NPs, this platform may improve current therapeutic approaches and reduce dosage-related side effects to achieve better clinical outcomes in OS patients.

**Keywords:** Tyrosine kinase inhibitor, Ponatinib, Osteosarcoma, Biomimicry, Nanoparticle, Drug delivery system

## Graphical Abstract



## Introduction

Over the last few years, the introduction of targeted anticancer drugs has revolutionized therapy for many tumors (Lee et al. 2018). Specifically, small-molecule tyrosine kinase inhibitors (TKIs) enable the targeting of specific signaling pathways contributing to cancer progression (Huang et al. 2020). Ponatinib (Pon) is a Food and Drug Administration (FDA)-approved TKI used against specific subsets of chronic myeloid leukemia and acute lymphoblastic leukemia (Massaro et al. 2018), and is currently being investigated for a variety of other neoplasms including biliary cancer, non-small cell lung cancer, and gastrointestinal stromal tumors (Tan et al. 2019). Pon inhibits several different signaling pathways upregulated in a range of neoplasms, including Src (Hu et al. 2015; Urciuoli et al. 2018; Evola et al. 2017), which is a critical oncogenic pathway in osteosarcoma (OS) development and progression that has been reported to be of prognostic relevance in patients' survival (Rathore et al. 2021; Sevelde et al. 2015; Xu et al. 2018; Guan et al. 2020; Zamborsky et al. 2019; Zhao et al. 2021). However, the FDA has issued a black box warning due to Pon's severe vascular adverse effects in 27% of treated patients (US FDA 2013; Musumeci et al. 2018). Free Pon administration also causes significant thrombocytopenia and neutropenia in 37% and 19% of patients, respectively (Cortes et al. 2014; De Lin et al. 2017). These drawbacks have severely limited Pon application for many other tumors. Therefore, improving targeting and reducing dosage and side effects would allow re-evaluation of this drug for cancer therapy.

OS is the most common malignant primary bone tumor, with roughly 1000 new cases yearly in the USA, and represents 2% of all pediatric tumors (Zhao et al. 2021; Harrison et al. 2018). The prognosis depends on the extent of the disease at diagnosis, with a 5-year survival of around 70% for localized tumors, but only 20–30% for distal metastatic OS (Janeway and Grier 2010; Picci et al. 1994; Gill et al. 2021). Its treatment relies on a combination of surgery and chemotherapy (Harrison et al. 2018; Picci et al. 1994; Gill et al. 2021). The gold standard chemotherapy in pediatric OS is a combination of doxorubicin, cisplatin, and a high dose of methotrexate (called the MAP protocol) (Whelan et al. 2015; Eilber et al. 1987; Misaghi et al. 2018). Despite its therapeutic efficacy, MAP causes severe side effects and is frequently unable to definitively eradicate metastatic disease, which is the major cause of treatment failure and tumor relapse. Thus, drug resistance and dose-limiting toxicities are significant barriers for OS treatment (Hattinger et al. 2021; Wood et al. 2021), and there is still a dire need for therapies that can address this unmet clinical need.

To reduce the cytotoxicity and improve the therapeutic efficacy of various drugs, different nanoparticle (NPs) formulations have been developed as drug delivery systems (DDSs), and many of them are now successfully used in clinical practice (Anselmo and Mitragotri 2019; Cheng et al. 2021). Among these, some DDSs specifically deliver TKIs (Russo et al. 2021; Zhou et al. 2020), including Pon. However, these were the first attempts of delivery without a relevant animal model, neither a target tissue strategy (Smidova et al. 2021).

To address this, our laboratory developed and characterized biomimetic NP platforms. We first developed liposomes NPs formulated with biomimetic phospholipids (Lipo) that recapitulate the major components of cells' membrane [cholesterol, dipalmitoylphosphatidylcholine (DPPC) and 1,2-dioleoyl-sn-glycerol-3-phosphocholine

(DOPC)], and then we functionalized these NPs with leukocyte-derived membrane proteins, named leukosomes (Leuko) (Corbo et al. 2017a; Molinaro et al. 2018).

The presence of cells' membrane proteins on the surface of synthetic NPs conferred the biological identity and function of the cells from which they are derived introducing a second level of biomimicry. Specifically, leukocyte membrane proteins (e.g., CD45, CD47) enable long circulation time by avoiding immune clearance by the mononuclear phagocyte system (MPS) and provide an active targeting strategy employing lymphocyte function-associated antigen 1 (LFA-1), macrophage-1 antigen (Mac-1), and P-selectin glycoprotein ligand-1 (PSGL-1) to deliver the payload to both tumor-associated vasculature and parenchyma (Molinaro et al. 2016a; Zinger et al. 2021; Martinez et al. 2018). Given the unique properties of biomimetic NPs (Zhang et al. 2020; Sushnitha et al. 2020; Pasto et al. 2019), including multiple functional capabilities, tunable sizes, and high surface-area-to-volume ratio, they have shown great potential in various medical applications and management of a wide range of inflammation-associated pathologies, including inflammatory bowel disease, rheumatoid arthritis, infection, sepsis, and cancer (Zinger et al. 2021; Corbo et al. 2017b; Molinaro et al. 2019, 2020a, b; Boada et al. 2020).

We previously demonstrated that our biomimetic NPs can be reproducibly and efficiently loaded with Pon (Lipo and Leuko Pon) using bovine serum albumin (BSA) as a carrier protein to increase Pon solubility (Zinger et al. 2020; Fernandes et al. 2018). To address the challenges of OS therapy, we present our set of biomimetic NPs as new tools to attenuate OS development and progression. Herein, leveraging on the successful encapsulation of Pon into our NPs (Zinger et al. 2020), we report an alternative approach that could effectively reduce Pon toxicity, and achieve better tumor accumulation through Leuko-mediated active targeting of the inflamed OS stroma.

Therefore, we propose our biomimetic NPs as a vehicle for Pon delivery to enhance, tumor accumulation, and reduce dosage and toxic side effects *in vitro* and *in vivo*. Thus, our optimized DDS invites the re-evaluation of this already FDA-approved drug in the arsenal of pharmacological treatment for OS.

## Results

### Ponatinib and nanoparticles physiochemical properties

To identify promising small molecules for the treatment of high-risk bone tumors, including Ewing sarcoma and OS, we performed an unbiased high-throughput screen on sarcoma spheroids, which are a surrogate for self-renewal or stem cell properties, using the FDA-approved NCI Drug Set V small molecule library (Table 1). As shown in Additional file 1: Fig. S1, we assessed proof of principle single-concentration drug discovery screenings of up to 114 compounds and we identified several drugs with the ability to drastically reduce the viability and stem-like properties of bone sarcoma, including several chemotherapies such as doxorubicin and etoposide (Rothenaigner et al. 2021; Al Shihabi et al. 2021). We also identified Pon as being highly effective at targeting OS spheroids formation using the metastatic human 143B OS cell line (Additional file 1: Fig. S1). We chose to further study this compound due to its ability to target multiple key oncogenic signaling cascades in OS. If the drug's significant systemic prothrombotic side effects could be mitigated would offer a needed therapeutic option for high-risk OS

**Table 1** List of compounds NCI Approved Oncology Drug Set V

Name	Library set	Concentration (mM)	Activity
Hydroxyurea	NCI Approved Oncology Drug Set V	10	RNA inhibitor
Temozolomide	NCI Approved Oncology Drug Set V	10	DNA alkylating agent
Carmustine	NCI Approved Oncology Drug Set V	10	Alkylating agent
Ifosfamide	NCI Approved Oncology Drug Set V	10	Alkylating agent
Anastrozole	NCI Approved Oncology Drug Set V	10	Aromatase inhibitor
Pipobroman	NCI Approved Oncology Drug Set V	10	Alkylating agent
Axitinib	NCI Approved Oncology Drug Set V	10	Tyrosine kinase inhibitor
Dasatinib	NCI Approved Oncology Drug Set V	10	Tyrosine kinase inhibitor
Vandetanib	NCI Approved Oncology Drug Set V	10	Kinase inhibitor
Ponatinib	NCI Approved Oncology Drug Set V	10	RTK inhibitor
Allopurinol	NCI Approved Oncology Drug Set V	10	Purine analog, purine synthesis inhibitor
Busulfan	NCI Approved Oncology Drug Set V	10	DNA alkylating agent
Cyclophosphamide	NCI Approved Oncology Drug Set V	10	Alkylating agent
Cisplatin	NCI Approved Oncology Drug Set V	10	DNA crosslinking agent
Letrozole	NCI Approved Oncology Drug Set V	10	Aromatase inhibitor
Megestrol acetate	NCI Approved Oncology Drug Set V	10	Progestin
Mitoxantrone	NCI Approved Oncology Drug Set V	10	Topo II inhibitor
Pazopanib hydrochloride	NCI Approved Oncology Drug Set V	10	Tyrosine kinase inhibitor
Vemurafenib	NCI Approved Oncology Drug Set V	10	RAF/MEK inhibitor
Cabozantinib	NCI Approved Oncology Drug Set V	10	RTK inhibitor
Fluorouracil	NCI Approved Oncology Drug Set V	10	Thymidylate synthesis inhibitor (antimetabolite)
Altretamine	NCI Approved Oncology Drug Set V	10	Alkylating agent
Uracil mustard	NCI Approved Oncology Drug Set V	10	Alkylating agent
Tretinoin	NCI Approved Oncology Drug Set V	10	ATRA
Lenalidomide	NCI Approved Oncology Drug Set V	10	(Unknown, alter cytokine production)
Bendamustine hydrochloride	NCI Approved Oncology Drug Set V	10	Alkylating agent
Pemetrexed	NCI Approved Oncology Drug Set V	10	Folate antimetabolite
Imatinib	NCI Approved Oncology Drug Set V	10	Tyrosine kinase inhibitor

**Table 1** (continued)

Name	Library set	Concentration (mM)	Activity
Regorafenib	NCI Approved Oncology Drug Set V	10	RTK inhibitor
Bosutinib	NCI Approved Oncology Drug Set V	10	RTK inhibitor
Thiouanine	NCI Approved Oncology Drug Set V	10	Purine analog (antimetabolite)
Floxuridine	NCI Approved Oncology Drug Set V	10	Antimetabolite
Cytarabine hydrochloride	NCI Approved Oncology Drug Set V	10	DNA/RNA synthesis inhibitor
Dexrazoxane	NCI Approved Oncology Drug Set V	10	EDTA derivative
Pomalidomide	NCI Approved Oncology Drug Set V	10	Immunomodulator
Fludarabine phosphate	NCI Approved Oncology Drug Set V	10	Purine analog (antimetabolite)
Gefitinib	NCI Approved Oncology Drug Set V	10	EGFR inhibitor
Sorafenib	NCI Approved Oncology Drug Set V	10	Tyrosine-raf- and ser/thr kinase inhibitor
Idarubicin hydrochloride	NCI Approved Oncology Drug Set V	10	Anthracycline
Daunorubicin hydrochloride	NCI Approved Oncology Drug Set V	10	RNA/DNA synthesis inhibitor
Mercaptopurine	NCI Approved Oncology Drug Set V	10	DNA/RNA synthesis inhibitor
Methoxsalen	NCI Approved Oncology Drug Set V	10	Furanocoumarins
Thalidomide	NCI Approved Oncology Drug Set V	10	(unknown, alter cytokine production)
Pentostatin	NCI Approved Oncology Drug Set V	10	Antimetabolite
Chlorambucil	NCI Approved Oncology Drug Set V	10	Alkylating agent
Bortezomib	NCI Approved Oncology Drug Set V	10	Proteasome inhibitor
Vismodegib	NCI Approved Oncology Drug Set V	10	GLI1/GLI2 inhibitors
Raloxifene	NCI Approved Oncology Drug Set V	10	SERM
Nilotinib	NCI Approved Oncology Drug Set V	10	RTK inhibitor
Doxorubicin hydrochloride	NCI Approved Oncology Drug Set V	10	DNA intercalating agent
Mechlorethamine hydrochloride	NCI Approved Oncology Drug Set V	10	DNA alkylating agent
Lomustine	NCI Approved Oncology Drug Set V	10	Alkylating agent
Procarbazine hydrochloride	NCI Approved Oncology Drug Set V	10	Alkylating agent
Nelarabine	NCI Approved Oncology Drug Set V	10	DNA synthesis inhibitor
Mitomycin	NCI Approved Oncology Drug Set V	10	DNA crosslinking agent
Capecitabine	NCI Approved Oncology Drug Set V	10	Pyrimidine analogue

**Table 1** (continued)

Name	Library set	Concentration (mM)	Activity
Crizotinib	NCI Approved Oncology Drug Set V	10	Protein kinase inhibitor
Afatinib	NCI Approved Oncology Drug Set V	10	Angiokinase inhibitor
Ixabepilone	NCI Approved Oncology Drug Set V	10	MT stabilizing agent
Etoposide	NCI Approved Oncology Drug Set V	10	Topo inhibitor
Thiotepa	NCI Approved Oncology Drug Set V	10	DNA alkylating agent
Azacitidine	NCI Approved Oncology Drug Set V	10	Inhibitor of DNMTs
Streptozocin	NCI Approved Oncology Drug Set V	10	Alkylating agent
Vorinostat	NCI Approved Oncology Drug Set V	10	HDAC inhibitor
Mitotane	NCI Approved Oncology Drug Set V	10	Unknown (interferes with steroid synthesis)
Celecoxib	NCI Approved Oncology Drug Set V	10	Cox-2 inhibitor
Methotrexate	NCI Approved Oncology Drug Set V	10	Antimetabolite
Pralatrexate	NCI Approved Oncology Drug Set V	10	Antimetabolite
Romidepsin	NCI Approved Oncology Drug Set V	10	HDAC inhibitor
Tamoxifen citrate	NCI Approved Oncology Drug Set V	10	Anti-ER compound
Aminolevulinic acid hydrochloride	NCI Approved Oncology Drug Set V	10	Involved in porphyrin synthesis, used as a photodynamic therapy
Decitabine	NCI Approved Oncology Drug Set V	10	Inhibitor of DNMTs
Cladribine	NCI Approved Oncology Drug Set V	10	Purine analog (DNA synthesis inhibitor)
Exemestane	NCI Approved Oncology Drug Set V	10	Aromatase inhibitor
Clofarabine	NCI Approved Oncology Drug Set V	10	Nucleoside antimetabolite
Sunitinib	NCI Approved Oncology Drug Set V	10	RTK inhibitor
Topotecan hydrochloride	NCI Approved Oncology Drug Set V	10	Topo inhibitor
Enzalutamide	NCI Approved Oncology Drug Set V	10	Androgen receptor inhibitor
Omacetaxine mepesuccinate	NCI Approved Oncology Drug Set V	10	Protein translation inhibitor
Epirubicin hydrochloride	NCI Approved Oncology Drug Set V	10	DNA intercalating agent
Estramustine phosphate sodium	NCI Approved Oncology Drug Set V	10	Depolymerizes MTs, also metabolized to E2 and E1 in the liver
Carfilzomib	NCI Approved Oncology Drug Set V	10	Proteasome inhibitor
Dactinomycin	NCI Approved Oncology Drug Set V	10	RNA PolII inhibitor

**Table 1** (continued)

Name	Library set	Concentration (mM)	Activity
Dacarbazine	NCI Approved Oncology Drug Set V	10	Alkylates DNA
Melphalan hydrochloride	NCI Approved Oncology Drug Set V	10	DNA alkylating agent
Lapatinib	NCI Approved Oncology Drug Set V	10	Tyrosine kinase inhibitor
Docetaxel	NCI Approved Oncology Drug Set V	10	Taxane (MT stabilizer)
Plicamycin	NCI Approved Oncology Drug Set V	10	(Mithramycin) RNA synthesis inhibitor
Arsenic trioxide	NCI Approved Oncology Drug Set V	10	APL treatment (in combination with ATRA)
Abiraterone	NCI Approved Oncology Drug Set V	10	CYP17 inhibitor (reduces testosterone levels)
Irinotecan hydrochloride	NCI Approved Oncology Drug Set V	10	Topo I inhibitor
Cabazitaxel	NCI Approved Oncology Drug Set V	10	Taxol derivative
Bleomycin sulfate	NCI Approved Oncology Drug Set V	10	DNA breaks
Triethylenemelamine	NCI Approved Oncology Drug Set V	10	DNA alkylating agent
Fulvestrant	NCI Approved Oncology Drug Set V	10	SERM
Paclitaxel	NCI Approved Oncology Drug Set V	10	MT stabilizer
Vinorelbine tartrate	NCI Approved Oncology Drug Set V	10	MT inhibitor
Carboplatin	NCI Approved Oncology Drug Set V	10	DNA intercalating agent
Trametinib	NCI Approved Oncology Drug Set V	10	MEK inhibitor
Vinblastine sulfate	NCI Approved Oncology Drug Set V	10	MT inhibitor
Temsirolimus	NCI Approved Oncology Drug Set V	10	mTOR inhibitor
Erlotinib hydrochloride	NCI Approved Oncology Drug Set V	10	Tyrosine kinase inhibitor (EGFR specific)
Dabrafenib mesylate	NCI Approved Oncology Drug Set V	10	ATP-competitive kinase inhibitor and targets the MAPK pathway
Vincristine sulfate	NCI Approved Oncology Drug Set V	10	MT disruptor
Gemcitabine hydrochloride	NCI Approved Oncology Drug Set V	10	(Nucleoside analog) inhibits DNA synthesis
Amifostine	NCI Approved Oncology Drug Set V	10	DNA intercalating agent
Teniposide	NCI Approved Oncology Drug Set V	10	Topo II inhibitor
Sirolimus	NCI Approved Oncology Drug Set V	10	(Rapamycin) mTOR inhibitor
Imiquimod	NCI Approved Oncology Drug Set V	10	TLR7 agonist
Zoledronic acid	NCI Approved Oncology Drug Set V	10	Bisphosphonate (prevents bone resorption)

**Table 1** (continued)

Name	Library set	Concentration (mM)	Activity
Valrubicin	NCI Approved Oncology Drug Set V	10	Topo II inhibitor
Everolimus	NCI Approved Oncology Drug Set V	10	mTOR inhibitor
Plerixafor	NCI Approved Oncology Drug Set V	10	CXCR4 blocker
Oxaliplatin	NCI Approved Oncology Drug Set V	10	DNA synthesis inhibitor

Screening data from the Approved Oncology Drug Set V Library

patients. We also decided to prioritize our studies in OS, versus Ewing sarcoma, due to the greater availability of patient-derived xenograft models and our syngeneic murine OS models that allow for more comprehensive targeting and therapeutic studies using immunocompetent models.

Pon, a multi-TKI of Src, Abl, and vascular endothelial growth factor receptor (VEGFR), is characterized by very poor water solubility, thus hindering its encapsulation in nanoformulations. To address this limitation, we used BSA as a carrier to encapsulate Pon into our Leuko and Lipo NPs, using empty NPs of each type as control, as shown in our previous publication (Zinger et al. 2020). NPs were formulated with a protein:lipid ratio of 1:40 (w/w) in order to achieve the slowest percentage drug released and the highest concentration of leukocyte proteins within the formulation (Zinger et al. 2021). Empty and Pon-loaded Leuko and Lipo NPs showed an average size of 140.8 nm, polydispersity index (PDI) of 0.1281 a.u., zeta potential (ZP) of  $-4.1563$  mV, NP concentration of  $4.37592E+12$  (particles/ml), and encapsulation efficiency of (8%) (Additional file 1: Fig. S2), confirming that presence of Pon and membrane proteins did not affect NP properties as we previously demonstrated (Zinger et al. 2020). NPs also exhibited remarkable stability in phosphate-buffered saline (PBS), showing an average size of 131.85 nm, PDI of 0.1554 a.u., ZP of  $-3.8115$  mV, and NP concentration of  $6.07563E+12$  (particles/ml) that were maintained when stored at  $4^{\circ}\text{C}$  up to 14 days (Additional file 1: Fig. S3).

#### **Biomimetic NPs internalization in murine and human osteosarcoma cell lines in vitro**

Demonstrating the efficient internalization of NPs by cells is of paramount importance to assess each formulation's ability to deliver its therapeutic payload to the target tissue; therefore, we assessed the interaction of biomimetic NPs with both murine and human OS cell lines in vitro. First, we treated murine OS (mOS) cells originated from primary OS (577 and F420) and metastatic lung tumor (RF379) and human PDX-derived OS (hOS) cells (TCCC-OS94 primary and TCCC-OS202 recurrency tumor) with empty Lipo and Leuko NPs to determine the maximum tolerable concentration, which was  $\sim 1.3 \times 10^{11}$  (corresponding to approximately  $\sim 0.1$ – $0.2$  mM lipid concentration) as reported in Additional file 1: Fig. S4. Then, we incubated all the cell lines with rhodamine-PE-labeled NPs ( $3 \times 10^{11}$  particles/ml). In all the tested cell lines, the NP uptake tended to increase over time (Fig. 1; Additional file 1: Figs. S5, S6). Specifically, we observed  $< 10\%$  NP uptake at 3 and 6 h after treatment (Additional

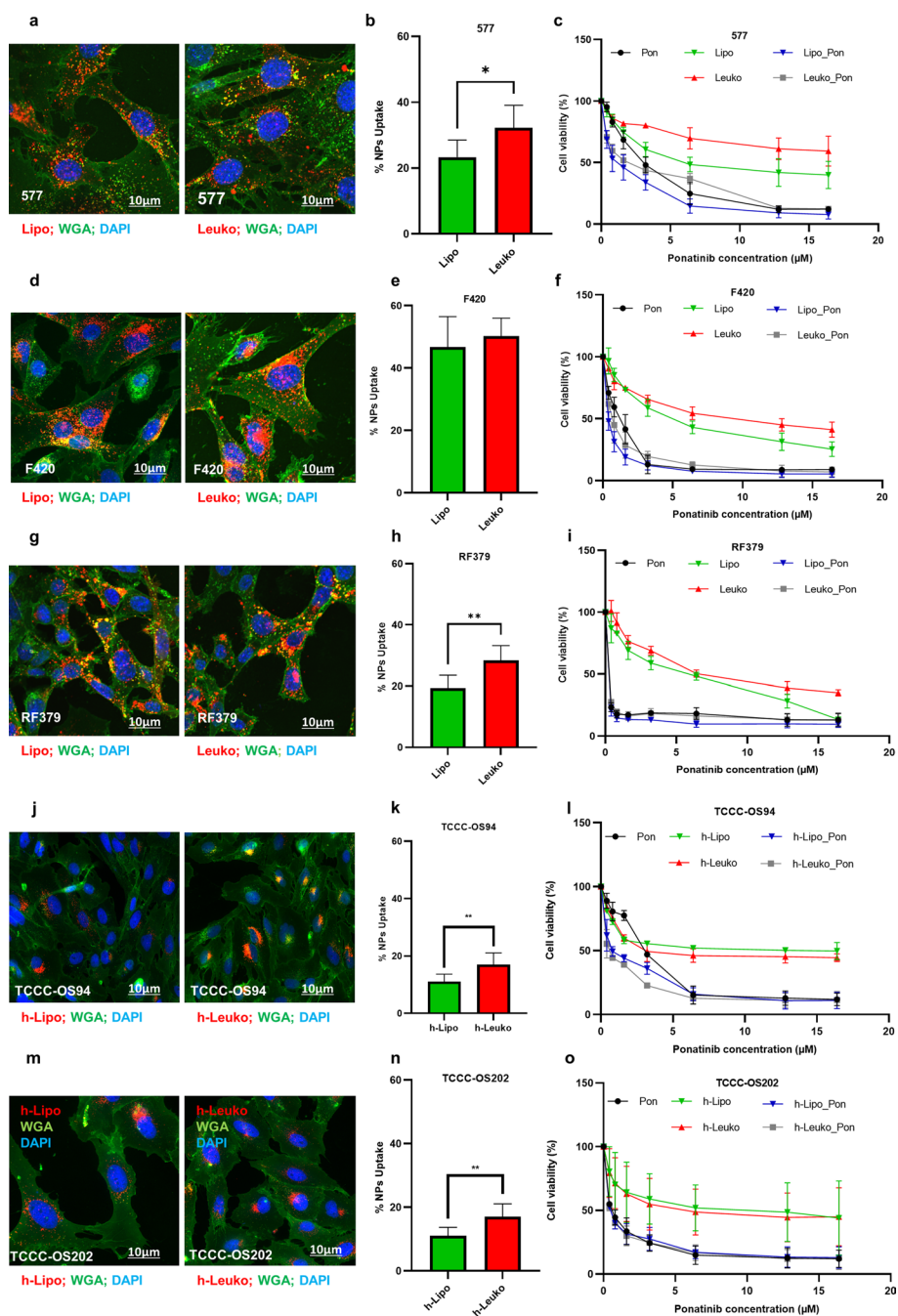


**Fig. 1** 2D biomimetic NP uptake and cytotoxicity on murine and human-derived OS cell lines. Representative images of NPs (Lipo and Leuko rhodamine labeled) internalization in murine (577, F420, RF379) (**a, d, g**) and human PDX-derived OS cells (TCCC-OS94, TCCC-OS202) (**j, m**) after 24-h treatment were observed using a Keyence BZ-X800 All-in-One Fluorescence Microscope. Merged images of green (FITC-WGA staining), blue (Dapi, nuclei staining), and red (rhodamine-NP staining) channels are shown. Scale bar = 10 μm. Relative uptake quantification of Lipo and Leuko in mOS (**b, e, h**) and in PDX-derived OS (**k, n**) cell lines after 24-h treatment. Ten images were analyzed for each condition. \*\* $p < 0.01$ ; \*\*\* $p < 0.001$ ; \*\*\*\* $p < 0.0001$ . Cell cytotoxicity analysis (MTT assay) of mOS (**c, f, i**) and hOS (**l, o**) exposed for 72 h to increasing concentrations of Pon, empty NP (Lipo and Leuko), and NP-loaded Pon (Lipo Pon, Leuko Pon). All data are expressed as mean  $\pm$  SD ( $n = 3$ ). Lipo and Leuko NPs for mOS, h-Lipo and h-Leuko NPs for human PDX-derived OS cells

file 1: Figs. S5, S6) while NP internalization increased 24-h post-treatment: 577 cells displayed 26% and 32%, RF379 22% and 26%; and F420 42% and 46% Lipo and Leuko uptake, respectively (Fig. 1a, b, d, e, g, h). NP uptake in human-derived PDX OS cell lines was lower: 11% for Lipo and 17% for Leuko in TCCC-OS94, while 9% uptake for Lipo and 16% for Leuko was observed in TCCC-OS202 at 24 h (Fig. 1j, k, m, n). Overall, all mOS and hOS cells showed a slightly to significantly higher uptake of Leuko depending on the cell lines. Conversely, only the F420 cell line did not demonstrate significant differences between Lipo and Leuko NP uptake at 24 h (Fig. 1e). As shown by immunofluorescence (Additional file 1: Figs. S5, S6), both Lipo and Leuko revealed a punctate cytosolic pattern at early time points, suggesting an endocytosis-mediated uptake, which changed at 24 h, when NP accumulation mostly appeared in the perinuclear region depending on the cell line (Fig. 1). Taken together, these data show that mOS and hOS cells efficiently uptake Lipo and Leuko NPs over time.

#### Anticancer efficiency of ponatinib-loaded biomimetic NPs against murine and human osteosarcoma cell lines in the 2D system

Considering the efficient NP internalization observed in all the mOS and hOS cell lines, our next step was to investigate the cell viability after Pon-loaded NP treatment to better assess anticancer efficacy *in vitro*. First, we evaluated the Pon  $IC_{50}$  dose (Additional file 1: Fig. S5) by exposing mOS and hOS cells to increasing concentrations of free Pon for 72 h. We found that Pon was able to suppress 577, F420, and RF379 cell viability by 50% at 3  $\mu$ M, 1.2  $\mu$ M, and 0.15  $\mu$ M doses, respectively (Additional file 1: Fig. S5a, b, c). For hOS cell lines, Pon  $IC_{50}$  doses were 3.8  $\mu$ M and 1.67  $\mu$ M for TCCC-OS94 and TCCC-OS202, respectively (Additional file 1: Fig. S5d, e), thus demonstrating comparable sensitivities between the murine and human OS cell lines. Subsequently, we tested the ability of Pon to kill mOS and hOS cells when encapsulated in NPs. In toxicity studies, a single exposure to Pon-loaded Lipo and Leuko showed a similar loss of survival compared to free Pon, as detected after 72 h (Fig. 1c, f, i, l, o;  $IC_{50}$  reported in Table 2). By contrast, treatment with equivalent amounts of empty Lipo and Leuko (equivalent particle concentrations used for loaded NPs) did not show toxic effect, in particular at the concentrations corresponding to Pon  $IC_{50}$  dose, only 10–15% of cell death was observed, reflecting the desired safety profiles of the NPs due to their biocompatible and biodegradable nature (Fig. 1c, f, i, l, o). These results suggest that empty NPs exhibit non-cytotoxic effects and only the delivery of Pon is affecting cell viability.

**Table 2** Ponatinib  $IC_{50}$  value

	577	F420	RF379	TCCC-OS94	TCCC-OS202
Pon ( $\mu$ M)	3	1.2	0.15	3.8	1.67
Lipo_Pon ( $\mu$ M)	1.1	0.3	0.05	2.87	0.88
Leuko_Pon ( $\mu$ M)	1.45	0.6	0.06	1.70	0.86

Cytotoxicity ( $IC_{50}$  values,  $\mu$ M) following 72-h exposure to Pon, Lipo and Leuko Pon-loaded NPs in a panel of murine OS (577, F420, RF379) and human PDX-derived OS (TCCC-OS94, TCCC-OS202) cell lines

### **Biomimetic NP internalization in murine and human osteosarcoma cell lines in 3D in vitro system**

The ability of drug-loaded NPs to reach their target cells may be affected by the complex physiology and architecture of the tissue. Three-dimensional tumor spheroids can recapitulate some aspects of this complexity, enabling high resolution when evaluating NPs penetration. Thus, we first optimized 3D spheroid growth of mOS and hOS cells and then evaluated the internalization and penetration of Lipo and Leuko rhodamine-PE-labeled NPs 24 h after treatment. With regard to mOS cells, only 577 and RF379 were able to form spheroids. As previously reported, cancer cells have different capacities to form spheroids, even for the same tumor type (Han et al. 2021). mOS and hOS cell lines formed tight spheroids in 2–3 days showing a defined border with an average diameter of 350  $\mu\text{m}$  ( $\pm 15$ ) at day 3. Spheroid formation was highly reproducible and variation in size on day 3 was  $\text{CV} \leq 5\%$  (data not shown).

When OS spheroids were incubated with rhodamine-PE-labeled NPs, we observed a higher accumulation of Leuko compared to Lipo at 24 h (Fig. 2). In particular, in the murine 577-derived spheroids, we detected 60% internalization of Leuko vs. 30% Lipo, and in the RF379 30% Leuko vs. 10% Lipo (Fig. 2a, b, d, e). For human-derived PDX spheroids, accumulation was overall slightly lower at these time points, showing 15% Leuko internalization vs. 3% Lipo for TCCC-OS94 and 8% Leuko vs. 4% Lipo for TCCC-OS202 (Fig. 2g, h, j, k). The confocal cross-sections (z-stack) showed penetration up to 60–80  $\mu\text{m}$  ( $\pm 10$ ) in depth, demonstrating the ability of these NPs to efficiently penetrate (Additional file 1: Figs. S8, S9).

The 3D results showed higher Leuko uptake and penetration by all OS cell lines compared to Lipo, thus providing greater rationale for the utility of our biomimetic NPs for targeting and effectively delivering cytotoxic agents.

### **Anticancer efficiency of ponatinib-loaded biomimetic NPs against murine and human osteosarcoma cell lines in the 3D system**

To address the effectiveness of NPs in delivering anti-tumor agents, we evaluated the anti-tumor effects of Pon NPs on mOS and hOS spheroids. As with the 2D monolayer, we first exposed spheroids derived from 577, RF379, TCCC-OS94, and TCCC-OS202 cells to increasing concentrations of free Pon for 72 h to establish the  $\text{IC}_{50}$  in the 3D model. We demonstrated that free Pon efficiently inhibits both mOS and hOS spheroid growth in a dose-dependent manner, as shown in the qualitative pictures and the 3D Cell Titer-Glo<sup>®</sup> viability assay (Additional file 1: Figs. S10, S11).

To further investigate the efficacy of Pon-loaded NPs, we exposed the spheroids to free Pon and Pon-loaded Lipo and Leuko NPs using  $\text{IC}_{50}$  and  $2 \times \text{IC}_{50}$  doses for 72 h. The results showed that the  $\text{IC}_{50}$  dose for both free Pon and Pon NPs was able to kill more than 50% of OS cells in 3D spheroids (Fig. 2). In particular, for 577 cells, the  $\text{IC}_{50}$  concentration (3  $\mu\text{M}$ ) of free Pon resulted in 40.9% reduction of viability, while Lipo Pon and Leuko Pon reduced viability 42% and 45%, respectively. Conversely, the  $2 \times \text{IC}_{50}$  (6  $\mu\text{M}$ ) treatment led to a 93 to 96% viability reduction for all free Pon, Lipo Pon and Leuko Pon (Fig. 2c). In RF379 cells, the  $\text{IC}_{50}$  (0.15  $\mu\text{M}$ ) of free Pon hindered cell viability by 51%, while Lipo Pon and Leuko Pon curtailed cell viability by 62% and 50%, respectively. The

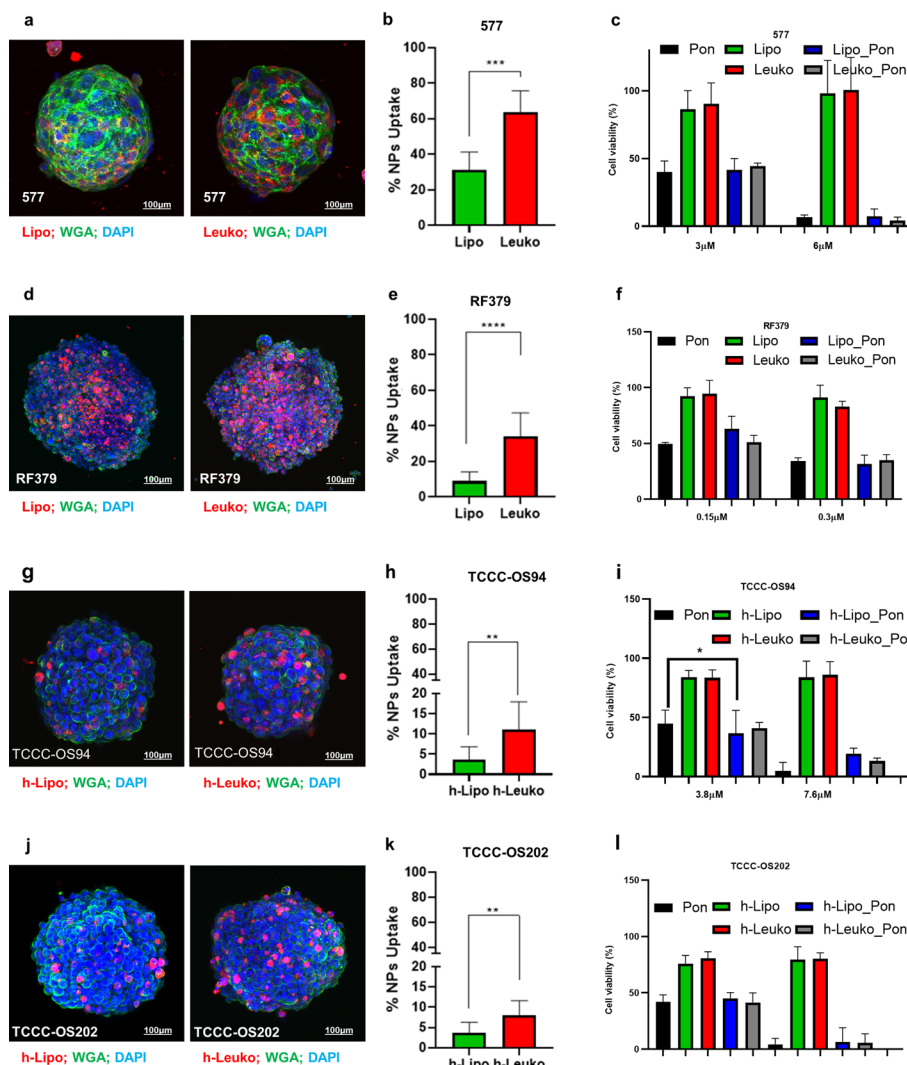


**Fig. 2** 3D biomimetic NP uptake and cytotoxicity on murine and human-derived OS cell lines. Representative images of Lipo and Leuko rhodamine-labeled NPs internalization at 24 h in mouse OS (577, RF379) (a, d) and PDX-derived OS (TCCC-OS94, TCCC-OS202) (g, j) cells using confocal Nikon A1 imaging system. Maximum projection images of green (FITC-WGA staining), blue (Dapi, nuclei staining), and red (rhodamine-NP staining) channels are shown. All data are expressed as mean ± SD (n = 8 spheroids per condition). Scale bar = 100 μm. Relative quantification of Lipo and Leuko NPs uptake in mOS (b, e) and hOS cells (h, k) spheroids after 24-h treatment. Cell cytotoxicity analysis (3D Cell Titer Glo assay) of mOS (c, f) and hOS (i, l) exposed for 72 h to increasing concentrations of Pon, empty NP (Lipo and Leuko), and NP-loaded Pon (Lipo Pon and Leuko Pon). All data are expressed as mean ± SD (n = 3). Lipo and Leuko NPs for mOS, h-Lipo and h-Leuko for human PDX-derived OS cells \*\*p < 0.01; \*\*\*p < 0.001; \*\*\*\*p < 0.0001

2 × IC<sub>50</sub> dose instead improved the treatment by reducing cell viability by 67%, 69%, and 65% for free Pon, Lipo Pon, and Leuko Pon, respectively (Fig. 2f).

In the hOS cell lines, Pon IC<sub>50</sub> (3.8 μM) treatment caused an 44% reduction in viability, while Lipo Pon and Leuko Pon achieved 37% and 41% decreases in TCCC-OS94. Doubling the dose to 2 × IC<sub>50</sub> (7.6 μM), we observed an improved treatment toxicity, leading free Pon, Lipo Pon, and Leuko Pon to reduce cell viability by 82–95% (Fig. 2i). Alternatively, in TCCC-OS202, the IC<sub>50</sub> (1.76 μM) and 2 × IC<sub>50</sub> (3.52 μM) treatment showed similar results. Spheroid viability was reduced by 42% with Pon, 45% with Lipo Pon, and

42% with Leuko Pon at the  $IC_{50}$  dose versus 95% with Pon, 93% with Lipo Pon, and 94% with Leuko Pon at the  $2 \times IC_{50}$  dose (Fig. 2L).

These results confirmed the ability of Pon-loaded NPs to kill OS cells with efficiency similar to or better than free Pon in 3D, with more than a 25% increase in Leuko Pon cytotoxic effects compared to the 2D system.

### **Biomimetic Leuko nanoparticle in vivo targeting**

As we previously published, Leuko NPs are able to avoid MPS uptake and increase circulation time in healthy mice (Corbo et al. 2017a), and to selectively adhere to the inflamed vasculature in breast tumors, local inflammation, atherosclerosis plaques and triple-negative breast cancer in comparison with the biomimetic Lipo (Molinaro et al. 2016a, 2018; Martinez et al. 2018). To study the effects of Pon biomimetic NPs and their targeting capability, we used an orthotopic OS mouse model. F420 OS cells ( $1 \times 10^6$ ) were injected into the tibia of C57BL/6 mice. After 2 weeks, when tumor formation was visible, Lipo and Leuko Cy7-labeled NPs were injected via tail vein. By IVM analysis (Fig. 3a, b), we noticed an increased accumulation of Leuko NPs in the tumor region and in the surrounding vessels compared to Lipo NPs 1-h post-injection. By imaging the NPs trafficking within the first 60 min, we also observed a different accumulation dynamic rate as shown in Fig. 3c Leuko targeted the tumor faster than Lipo ( $p < 0.0001$ ). This observation was also confirmed over time (1, 6, and 24 h) using the IVIS Lumina II System. In the tumor lesion, the strongest fluorescence signal was observed 1 h after injection (Fig. 3d), with greater targeting and preferential accumulation of Leuko compared to Lipo NPs as shown in the quantification graph (Fig. 3e). Moreover, the observed fluorescence intensity at the tumor site was much higher than in other organs (Fig. 3e, f); notably, Leuko accumulated less in the filtering organs compared to Lipo NPs, confirming the ability of the proteins' functionalization on Leuko NPs to enhance the targeting of the primary tumor. No noticeable organ damage or inflammatory lesions were observed in the H&E-stained sections of the major organs, suggesting that injected Lipo and Leuko NPs have no toxic effect (Fig. 3g).

### **Effect of ponatinib-loaded biomimetic NPs on OS tumor progression in vivo**

To investigate the efficacy of Pon NPs in OS mouse model, we first determined the tolerated dose and toxicity of free Pon in mice, comparing intravenous (IV) tail and intraperitoneal (IP) injections. Mice were injected with three doses of Pon: 20, 30, and 50 mg/kg. While Pon IV injections were immediately lethal for the mice (even at the lowest doses), Pon IP injections were well tolerated during 3 weeks of treatments (2 times per week) using 20 or 30 mg/kg Pon. The highest dose of Pon (50 mg/kg) started to show toxic effects after 2 weeks of treatments. Histopathology assessment was conducted in all cohorts and as shown in Fig. 4, drug-related toxic effects were observed in organs when free Pon was injected IV (Fig. 4a). These included, in particular in heart and lung, congested vessels and infiltration of inflammatory cells, mostly platelets that adhering to endothelial cells in the vessels can cause ischemia and thrombosis, the most common side effects of ponatinib. Abnormal morphology changes were also observed mostly in liver where microabscess (circle) involving a few hepatocytes with inflammatory cells and necrotic debris were present. When injected IP, toxic effects were observed at the

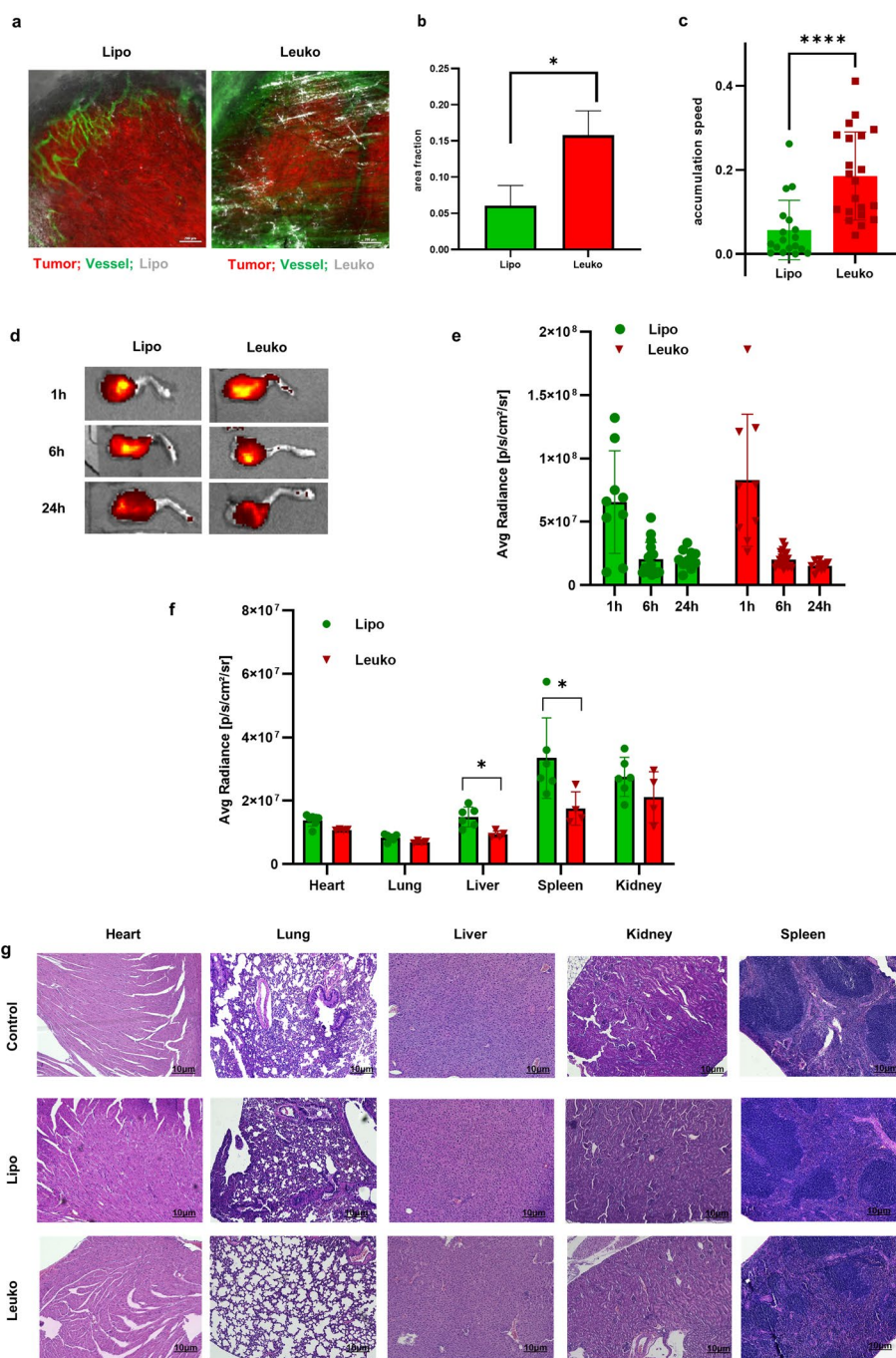


**Fig. 3** In vivo biomimetic NP targeting and biodistribution. Representative images of Lipo and Leuko NP accumulation within orthotopic osteosarcoma tumor after 1 h by IVM showing vessels (green), tumor cells (red) and NP (white) **(a)** and quantification of Lipo and Leuko accumulation within the tumors (Leuko in red, Lipo in green) **(b)** \**p* < 0.02. Lipo and Leuko NPs accumulation speed within the tumor in vivo during the first 60 min after injection as observed with IVM **(c)**. Representative fluorescent imaging of Lipo and Leuko Cy7-labeled NPs localization in the tumor after 1–6–24 h **(d)** and quantification of fluorescence intensity of regions-of-interest (ROI). (Leuko in red, Lipo in green) **(e)** \**p* < 0.05. Quantification of fluorescence intensity of regions-of-interest (ROI) of NP biodistribution in mice organs (Leuko in red, Lipo in green) **(f)**. \**p* < 0.05. Histological section of organs after 24 h of NP IV injections compared to control (no treatment). All sections were stained with hematoxylin–eosin **(g)**. Scale bar = 10 μm

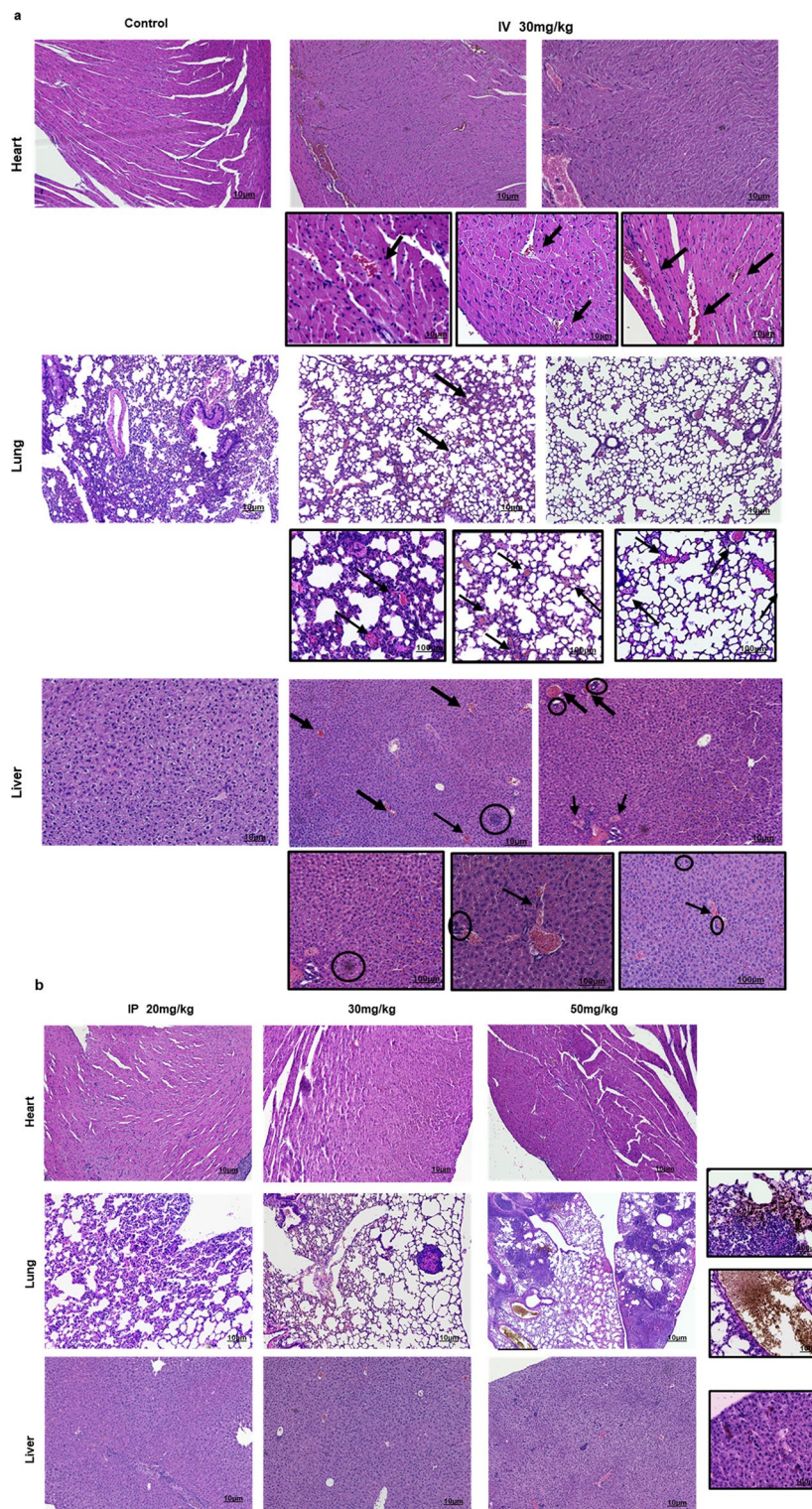


**Fig. 4** Ponatinib injection and toxicity. Histological section of mice heart, lung and liver after Pon IV (a) vs. IP (b) injections compared to control (no treatment). All sections were stained with hematoxylin–eosin. Mice were injected with Pon 2 times a week. Scale bar = 10 µm (highlighted frame scale bar = 100 µm, black arrow = immune cell infiltration, black circle area = necrotic area)

highest dose, 50 mg/kg Pon (apoptotic and infiltrating inflammatory cells, brown dots in Fig. 4b, highlighted frame).

To test the effect of Pon-loaded biomimetic NPs on tumor progression, OS-bearing mice were divided into six groups: (i) control, (ii) free Pon, (iii) empty Lipo, (iv) empty Leuko, (v) Lipo Pon, and (vi) Leuko Pon. Mice were treated 2 times a week for 3 weeks with 30 mg/kg Pon IP and 200  $\mu$ l NP IV (1.5 mg/kg Pon-loaded NPs). While untreated control mice and mice injected with empty NPs were killed within 2 weeks of treatment secondary to tumor size reaching study endpoint ( $>1000$  mm<sup>3</sup>) (Additional file 1: Fig. S14a), a slower tumor growth rate was observed in the other treatment groups (Fig. 5a). No significant difference was observed between mice treated with free Pon and Pon-loaded NPs as shown in the tumor cell fluorescence quantification graph in Fig. 5b. In addition to slowed tumor progression, the survival rate of the treated OS-bearing mice was higher compared to no treated mice ( $p < 0.05$ ) but no significant differences were observed among the treatment groups (Fig. 5c). No strong evidence of organ damage was observed in the major organs 3 weeks after treatments as shown in Fig. 5d. However, in Pon treatment group mice, we observed some infiltrating inflammatory cells (brown dots) in lung and liver.

Therefore, our results suggest that the Pon NPs' increased tumor targeting ability, reduced treatment dose (1.5 mg/kg loaded Pon vs. 30 mg/kg free Pon) while maintaining anti-tumor activity comparable to the higher dose of free drug. In fact, while 1.5 mg/kg Pon dose loaded into the biomimetic NPs were able to slow down the tumor growth, the corresponding amount of free drug injected IV, well tolerated by the mice, did not show any effect of tumor growth (Additional file 1: Fig. S14b). Thus, our approaches highlight the potential use of biomimetic NPs, specifically Pon NPs, as a future therapeutic treatment for OS.

## Discussion

In the last 20 years, many TKIs have entered clinical practice, improving treatment for cancers, including different types of sarcoma (Huang et al. 2020; Wilding et al. 2019; Nakano et al. 2018; Tian et al. 2020; Jiao et al. 2018). TKIs targeting angiogenesis-related kinases such as VEGFRs and Src, have been verified to be helpful in prolonging the progression-free survival of advanced OS patients (Tian et al. 2020; Gao et al. 2019). Unfortunately, some of these compounds present sub-optimal properties such as poor solubility, low oral bioavailability, and severe adverse effects, which limit their clinical application.

Among these TKIs, Pon, marketed as ICLUSIG<sup>®</sup>, is an orally active multi-tyrosine kinase inhibitor currently approved by the FDA for patients with chronic myeloid leukemia and Philadelphia chromosome-positive acute lymphoblastic leukemia (Molica et al. 2019; Hoy and Hoy 2014). Pon has shown significant efficacy towards adult malignancies, but its use in pediatric oncology has not been thoroughly assessed because of the reported detrimental systemic effects, including prothrombotic events and cardiotoxicities that have led to a "black box" warning from the FDA (US FDA 2013; Musumeci et al. 2018; Gainor and Chabner 2015). However, due to its ability to effectively target multiple oncogenic signaling cascades that are critical in pediatric malignancies, a Phase I/II trial (Clinicaltrials.gov: NCT03934372) was recently opened to evaluate the safety and

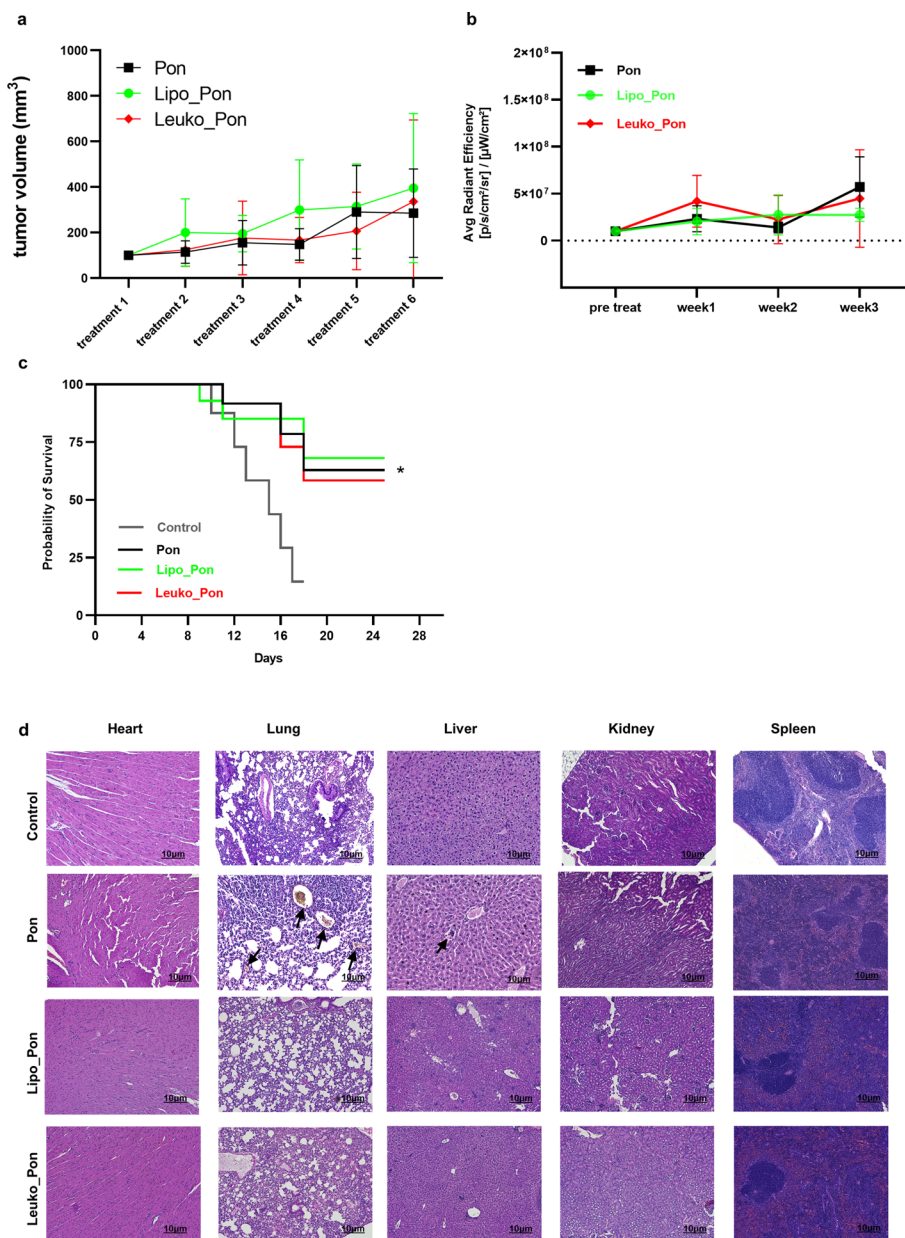


**Fig. 5** Ponatinib in vivo efficacy. Mouse tumor growth quantification (a), quantification of fluorescence intensity of regions-of-interest (ROI) by IVIS analyses (b), Kaplan–Meier survival (c) of mice treated with Pon (30 mg/ml, IP injections) and Pon NPs (1.5 mg/ml IV injections) 2 times per week, for 3 weeks. \* $p < 0.5$  Pon vs. control, Leuko Pon vs. control, Lipo Pon vs. control.  $n = 10$  mice for each group (Leuko in red, Lip green, Pon in black, control in grey). Histological section of mice organs after the 3 weeks of Pon, Leuko and Lipo Pon-loaded NPs treatment (d). All sections were stained with hematoxylin–eosin (black arrow = immune cell infiltration). Scale bar = 10  $\mu\text{m}$

efficacy of ponatinib for recurrent and refractory pediatric solid tumors and lymphoma. This trial highlights the potential value that safe and effective delivery of Pon can be a viable therapeutic option for pediatric oncology patients.

Even though Pon therapeutic potential remains high, the application of an efficient drug delivery system with disease-targeting moieties to improve targeting and reduce

potential Pon-associated side effects will help re-evaluating this drug for solid tumor treatments (Musumeci et al. 2018). Indeed, from our high-throughput screen of FDA-approved small molecules capable of inhibiting sarcoma spheroids development, we identified Pon as a possible therapeutic candidate.

It is worth noting that several nano-drug carriers have already been developed for OS therapy (Giordano et al. 2021), such as drug-loaded magnetic liposomes, chitosan–dipotassium orthophosphate hydrogel for doxorubicin delivery, dextran-centered lipid-modified polymeric NP conjugated with doxorubicin, doxorubicin-decorated magnetic liposomes, and multi-drug loaded NPs conjugated with zoledronic acid (Wang et al. 2020). However, all of these promising approaches were either associated with cytotoxic effects or low efficacy (Wang et al. 2020; Liu et al. 2021). In comparison, the biomimetic NPs used in the present work showed higher retention time in circulation, lower accumulation in the filtering organs (e.g., kidney, liver and spleen), increased targeting and drug accumulation in the tumor due to the physical–chemical feature. We previously demonstrated that Leuko-mediated delivery reduces drug toxicity, enhances targeted delivery, and improves drug bioavailability and pharmacokinetics (Corbo et al. 2017a; Molinaro et al. 2016a, 2018, 2020b; Martinez et al. 2018). Therefore, using our understanding of BSA as a carrier for Pon in the blood, we have successfully encapsulated Pon into our biomimetic NPs to repurpose it as an efficient and safe anticancer drug. While we were able to achieve only 8–10% Pon encapsulation efficiency, this dose was sufficient to show a therapeutic effect (Zinger et al. 2020). The presence of leukocyte adhesion membrane proteins (LEA-1, Mac-1, and PSGL-1) confers to Leuko NPs active targeting toward proteins expressed by inflamed blood vessels, the first physiological barrier that NPs encounter after intravenous administration (Zinger et al. 2021; Martinez et al. 2018). This property can be exploited for the treatment of primary and pulmonary metastatic OS, which are characterized by induced neovascularization and inflammatory cell accumulation (Buddingh et al. 2011; Joyce and Pollard 2009). Consequently, we assessed the anti-tumor efficacy of our NPs Pon formulations, demonstrating promising results against OS. Exploiting Leuko NP targeting of the inflamed endothelium in the proximity of OS cells (Molinaro et al. 2016b), we specifically delivered Pon to the tumor site, thereby addressing the limitation of bone structure accessibility and overcoming tumor microenvironment drug-resistance (Giordano et al. 2021).

We first demonstrated the ability of Pon-loaded biomimetic NPs to be efficiently internalized by both mOS and hOS cell lines *in vitro* (Fig. 1). We found that Leuko Pon was potently able to inhibit the viability of mOS and hOS cell lines with a similar or lower  $IC_{50}$  compared to free Pon and Lipo Pon, suggesting sustained drug release from Leuko Pon NPs while ensuring the same or greater cytotoxicity (Fig. 1). Although the cytotoxic effect of NPs Pon was the same or slightly greater than the free drug, this result could be explained by the incomplete release of Pon from NPs in the absence of an intratumoral acidic microenvironment in the *in vitro* setting, which lacks the complexity of the *in vivo* tumor microenvironment (Fernandes et al. 2018).

To achieve therapeutic efficacy, NPs need to penetrate and the payload (i.e., drug) effectively released and accumulate in the tumor. While animal models represent the best option to recapitulate tumor biology, 3D models have been proven to be more physiologically relevant than 2D monolayer cultures in recapitulating some key features of

solid tumors (e.g., kinetic growth, cell layers, oxygen gradient, lower pH) (Van Zundert et al. 2020) and allow tracking of NP penetration at the cellular level with high resolution (Tchoryk et al. 2019). Moreover, whereas few research groups have investigated NP trafficking in various spheroid tumor models, biomimetic NP penetration and efficacy have not previously been assessed in OS-derived spheroids. Consistent with prior results in 2D models, NPs were able to efficiently penetrate in both mOS- and hOS-derived spheroids at 24 h (Fig. 2), showing a higher percentage of Leuko uptake compared to Lipo because of the presence of membrane proteins that increase cell–cell interactions and promote targeting as we previously published (Molinaro et al. 2016a, 2020b; Martinez et al. 2018). In addition, using the same  $IC_{50}$  dosage determined in our 2D model, Leuko NPs efficiently delivered Pon into tumor spheroids, affecting OS cell viability with the same efficacy as free Pon and Lipo Pon. Thus, confirming the ability of Leuko Pon to maintain the same free drug efficacy, could in turn facilitate prolonged anti-tumor cytotoxicity and reduce the Pon dosage required in vivo. Also, the use of different mOS and hOS cell lines enables a more complete understanding of the effect of Pon NPs on tumor cells, mimicking the genetic heterogeneity found in OS patients (Wang et al. 2019).

Differences in NPs internalization and penetration between cancer cell lines have been widely reported, as the significant differences in the response of cell populations in 2D monolayer and 3D spheroid models. This is likely due to genetic and phenotypic heterogeneity between cell line populations, resulting in variation in cell size, packing density, membrane composition and intrinsic endocytic potential. These cellular properties, alongside with the physical and biological properties of NPs, modulate cell–particle interactions and affect internalization in dense tumors (Han et al. 2021; Xu et al. 2014). These experiments highlight the importance of these biological differences and their interplay with nanomaterials when exploring mechanisms of NPs uptake. Overall, we demonstrated the ability of NPs Pon to reach the same or slightly greater cytotoxicity as that of free Pon, while increasing targeting and reducing drug-related side effects in vivo.

While we did not observe a strong difference between Pon-loaded NPs and free Pon in cell-based models, of critical importance is the fact that our NPs platform could overcome Pon toxicity in vivo, as reported by FDA. Reducing the dosage needed for the treatment, these biomimetic NPs enable the repurposing of the drug for clinical application. In mice, we observed a fatal effect when Pon was administered IV, causing death within 1 hour, posing a tremendous limitation and leaving IP injection as the only tolerated solution (Fig. 4). Pon-loaded NPs, however, were not only well tolerated by the mice when injected IV but were also able to slow tumor growth and avoid Pon-related side effects (Fig. 5, Additional file 1: Fig. S13), demonstrating the therapeutic potential of Pon-loaded NPs. Remarkably, Leuko Pon efficiently accumulated into the tumor lesion in an OS orthotopic model 1-h post-injection, unlike Lipo Pon (Fig. 3). Thus, we demonstrated in vivo the ability of Leuko Pon biomimetic NPs to increase accumulation in the tumor stroma compared to Lipo NPs, while showing lower retention in the filtering organs responsible for NP clearance, including liver and spleen (Fig. 3) (Zinger et al. 2021; Molinaro et al. 2020b). Moreover we observed that the presence of membrane proteins also affects the targeting ability by increasing the accumulation rate of these biomimetic NPs compared to the Lipo formulation. In detail, exploiting the leukocytes' biological mechanism to be recruited to the site of inflammation, leukosomes

demonstrated increased targeting of inflamed endothelia (Martinez et al. 2018) and cancer vasculature and stroma. Despite not knowing the specific molecular mechanism involved in leukocyte recruitment to the tumor, it is a common feature of many neoplasms, including osteosarcoma (Liu et al. 2016), to elicit a chronic inflammatory environment in the diseased tissue, which results in local leukocytes chemotaxis” (Zinger et al. 2021; Molinaro et al. 2020b). These data suggested that the introduction of cells’ membrane protein on Leuko Pon induced a better tumor targeting in comparison with the bare lipidic NPs (Lipo).

Finally, the *in vivo* efficacy study demonstrated the ability of both biomimetic NPs to effectively slow tumor growth (Fig. 5). When comparing NPs Pon IV and free Pon IP, we observed similar tumor growth inhibition. The route of drug administration (IV vs. IP) can affect serum clearance, tissue distribution, and drug pharmacokinetics in mice (Guichard et al. 1998; Chang et al. 2010). IV delivery is the most efficient route for delivering substances to animals as it precludes delays associated with absorption processes and alterations due to pre-systemic effects, while remaining rapid and accurate. The major pharmacological problems with IP drug injection are the limited tissue penetration and poor homogeneity of drug distribution (Shimada et al. 2005) even though it results in faster and more complete absorption as well as resembles the metabolic fate compared to oral administration (the Pon route used in clinical setting) (Al Shoyaib et al. 2020; Lukas et al. 1971; Abu-Hijleh et al. 1995).

We also need to consider the differences in composition and structure of the free drug versus the drug loaded in NPs, as well as free drug interactions with other components in the blood that can affect the concentration of drug that reaches the tumor site (Guichard et al. 1998; Gao et al. 2016).

Several other factors need to be taken into consideration while evaluating drug kinetic and accumulation: blood flow, vascular structure, and vessel permeability, surrounding stroma, MPS function, and the type of tumor (Petschauer et al. 2015). Mathematical models, taking into consideration all these factors, have been employed to help to get a better understanding of the drug distribution as well as the pharmacokinetics but tumor models that accurately represent the types of tumors seen in patients are really as important too for conducting these informative studies from a preclinical perspective (Petschauer et al. 2015; Chen et al. 2021; Yao et al. 2018; Kovshova et al. 2021; Chu et al. 2013).

However, taking into consideration all of these factors and considering that the Pon dosage loaded into NPs was drastically lower (free Pon IP 30 mg/kg vs. Leuko Pon IV 1.5 mg/kg), Pon-loaded NPs are likely more effective than free Pon (Fig. 5). Therefore, optimization of Pon NPs to increase its encapsulated concentrations, together with the evaluation of Pon and Pon-loaded NPs pharmacokinetic profile could improve treatment outcome.

Overall, these results suggest that biomimetic NPs loaded with tyrosine kinase inhibitors can be a crucial tool for OS treatment; moreover, leukocyte-derived membrane proteins could increase the interaction of Leuko-mediated drug delivery in the inflamed tumor vasculature, as we also demonstrated in melanoma and breast cancer (Molinaro et al. 2020b). In addition, since conventional DDSs fail to deliver drugs at the effective concentration for cancer cell death due to the complexity of the tumor

microenvironment (Fernandes et al. 2018), Leuko Pon can be considered an alternative platform able to tune cell crosstalk within the inflamed OS tumor microenvironment (Joyce and Pollard 2009), thereby enhancing the accumulation of Pon at the tumor site and surrounding inflamed tissue. We believe that our biomimetic DDS could also re-educate the tumor environment which involves tumor cells, immune cells, stromal cell, to block the initiation of metastasis (Wang et al. 2020).

## Conclusion

In conclusion, biomimetic NPs efficiently enhanced tumor penetration and retention in vivo and maximized the activity of the encapsulated Pon for tumor therapy. In an immunocompetent murine model of OS, our Pon-loaded NPs were able to reduce tumor growth and prolong overall survival of the experimental group. These promising results suggest therapeutic potential for Pon biomimetic NPs for OS, not only for primary tumors but also for metastasis. In the future, biomimetic NPs could be expanded to deliver a large number of small-molecule inhibitors and easily applied across a wide range of solid tumor types, providing a meaningful strategy for reducing side effects and enhancing patient outcomes in the clinic.

## Materials and methods

### Reagents

Membrane protein extraction kit, chloroform, methanol, Tween 20, and 2-mercaptoethanol were purchased from Sigma-Aldrich (Missouri, United States). Dipalmitoylphosphatidylcholine (DPPC), 1,2-dioleoyl-sn-glycerol-3-phosphocholine (DOPC) and cholesterol (ovine wool, > 98%) were purchased from Avanti Polar Lipids, Inc. (Alabama, United States). Ponatinib (LC laboratories, Massachusetts, United States). Float-A-Lyzer G2 dialysis devices were purchased from Spectrum Laboratories (Massachusetts, United States). PBS 10× solution, acetonitrile (ACN) syringe filters 0.22 μm, sterile PVDF, MilliporeSigma Milli-Q Ultrapure Water Systems Accessory, and Pierce Rapid Gold BCA Protein Assay Kit were purchased from Fisher Scientific (Pennsylvania, United States). Dynamic Light Scattering (DLS), NanoSight NS300, and disposable cuvettes primarily for the measurement of ZP were provided from Malvern Instruments (Worcestershire, United Kingdom). Other supplies used included semi-microvolume disposable polystyrene cuvettes for size measurements (Biorad, California, United States), Waters 2695 high-performance liquid chromatography (HPLC) System w/UV Detector (Waters Corporation, Massachusetts, United States), Verex vial kit for HPLC and Luna<sup>®</sup> 5 μm C18(2) 100 Å, LC Column 250 × 4.6 mm (Phenomenex, California, United States), rotary evaporator (BUCHI Labortechnik AG, Flawil, Switzerland), centrifugal devices with Omega<sup>™</sup> Membrane 30K from (Pall Corporation, New York, United States), and FLUOstar Omega microplate reader (BMG, Labtech Ortenberg, Germany).

### Membrane protein extraction and quantification

Membrane proteins were extracted from murine monocytes/macrophages (J774 cells), or human monocytes (THP-1 cells) cell lines using a ProteoExtract Native Membrane Protein Extraction Kit according to the manufacturer's protocol and as we have already published in our previous works (Molinario et al. 2016a; Boada et al. 2020).

Quantification of the extracted protein concentration was determined using a Pierce Rapid Gold BCA Protein Assay Kit according to the manufacturer's protocol. Absorbance was measured at 480 nm on a FLUO star Omega microplate reader, and protein concentration was determined using a calibration curve with albumin diluted in 1× PBS at the following concentrations: 0, 25, 125, 250, 500, 750, 1000, and 1500 µg/ml.

#### **Nanoparticle preparation**

NPs were fabricated as described in our previous publications (Boada et al. 2020). In this work, we used Liposome (Lipo) as our control group and formulated Leukosome (Leuko) using either membrane proteins derived from J774 or THP-1 cells, referred to as Leuko and h-Leuko, respectively. Briefly, NPs were formulated using DPPC, DOPC, and cholesterol (molar ratio 4:3:3) dissolved in chloroform to a final lipid concentration of 9 mM. Once lipids were dissolved, they were mixed in a round bottom flask and chloroform was evaporated using the rotary evaporator (45 °C, 30 min, 0 psi, 280 rpm), and a thin film was obtained. For Lipo, the thin film was hydrated with 2 ml BSA dissolved in 1× PBS [200 mg/ml (w/v)] for 30 min, 45 °C, 280 rpm. For Leuko, membrane proteins were added at one-fortieth of the lipid weight and brought to 2 ml with BSA dissolved in 1× PBS. Lipo and Leuko formulations were extruded using different cycles of polycarbonate membranes (0.4, 0.2, and 0.08 µm) setting the heating system at 45 °C. Lipo Pon and Leuko Pon were fabricated using the same procedure, adding 2 mg Pon dissolved in methanol:chloroform 1:1 (v/v) during thin-film preparation. Fluorescent NPs were formulated as defined above, adding 0.1 mg rhodamine, Cy5.5, or Cy7 dissolved in chloroform during thin-film preparation. After extrusion, the samples were loaded inside the dialysis membranes and put in 2 L 1× PBS at 4 °C. Buffer was changed three times (after 1, 3, and 16 h). Samples were sterilized by loading in a syringe and using a 0.22 µm PVDF filter.

#### **Nanoparticle characterization and stability**

All NPs were characterized by size, polydispersity index (PDI), and zeta potential (ZP) with DLS measurements. Briefly, for evaluating size and PDI, polystyrene cuvettes were loaded with 495 µl 1× PBS and 5 µl sample 100:1 (v/v). Size and PDI were evaluated as an average of 30 measurements. The evaluation of ZP was done by loading 900 µl Milli-Q, 90 µl 1× PBS, and 10 µl sample into the disposable cuvettes. ZP was evaluated as an average of 45 measurements. NP concentration was evaluated using NanoSight NS300. The samples were diluted in Milli-Q water 1:10,000 (v/v) with the following parameters: temperature, 25 °C, screen gain, 1; camera level, 13; infusion rate, 100; and flow ratio, 1 ml/min. For each sample, five measurements were acquired with a duration of 60 s each. A detection threshold equal to 7 was used to calculate the final NP concentration. NPs were stored at 4 °C, and the size, PDI, and ZP measurements were repeated after 1, 4, 7, and 14 days, while NP concentration was measured after 1 and 14 days.

#### **Ponatinib encapsulation and stability**

Pon encapsulation was evaluated after nanoparticle filtration via HPLC analysis. 30 µl of the sample were mixed with 120 µl 1× PBS and 150 µl ACN into 1.5-ml Eppendorf tubes. The tubes were warmed for 10 min at 40 °C, then sonicated for 10 min at 40 °C.

The samples were centrifugated for 10 min at 17,000 rcf and 40 °C, and 200 µl of supernatant was transferred into the centrifugal filtering devices and centrifuged for 10 min at 17,000 rcf and 40 °C. Finally, Pon concentration was evaluated using HPLC. Pon encapsulation was also assessed at days 0, 4, and 7 for stability testing via HPLC analysis. Sample triplicates were aliquoted for each time point and stored at 4 °C in 1.5-ml ultracentrifuge tubes after filtration. At each time point, the samples were ultra-centrifuged for 60 min at 4 °C at 226,395 rcf. After ultracentrifugation, the supernatant was removed, and the pellet was resuspended in 1 × PBS to the initial volume.

#### **High-throughput screen using a library of FDA-approved compounds**

In collaboration with the Center for Drug Discovery at Baylor College of Medicine, a high-throughput screen was devised to identify small molecules that have activity against bone sarcoma tumor-initiating, or cancer stem cell-like properties. Briefly, 143B (OS) and TC71 (Ewing sarcoma) cells were seeded on ultra-low attachment 96-well plates (Corning®) at a density of  $4 \times 10^3$  viable cells in 100 µl of sarcosphere medium (B27: 1 ×, bFGF: 20 ng/ml, EGF: 20 ng/ml, DMEM/F12, without phenol red) per well using Multidrop Combi dispenser (Thermo Fisher Scientific, Inc.) on day 1. Sarcospheres were treated with compounds from the NCI approved Oncology Set V (114 compounds) at 10 µM on day 2 using a Tecan Freedom Evo Robotic System (Tecan Inc), and analyzed for cell viability using CellTiter-Glo® cell viability assay on day 5. The cell-killing effect of each compound was normalized to the viability of DMSO treated cells measured in parallel. Testing was done in triplicate.

#### **Cell lines**

Mouse Osteosarcoma cell lines 577 and F420 (primary), RF379 (lung metastasis), and human patient-derived xenograft (PDX) OS cells TCCC-OS94 (diagnostic primary lesion) and TCCC-OS202 (recurrent OS) were obtained from Dr. Jason T. Yustein (Texas Children's Cancer and Hematology Centers, Department of Pediatrics, Baylor College of Medicine, Houston, TX, USA). The murine cell lines were established from murine OS tumors generated in a conditional genetically engineered mouse model using an osteoblast-conditional CRE-recombinase model with alterations in p53, as previously described (Guichard et al. 1998). Patient-derived OS cells were established from pieces of fresh OS patient biopsy transplanted into multiple immune-defective mice to grow xenograft tumors (Chang et al. 2010). All cells were passaged for a maximum of 3 or 4 weeks, after which new seed stocks were thawed for experimental use. All cells were grown at 37 °C in 5% CO<sub>2</sub>. Murine OS cell lines were maintained as a subconfluent monolayer using high glucose Dulbecco's modified Eagle's medium (DMEM, Gibco) supplemented with 10% fetal bovine serum (FBS, Atlas Biologicals) and 1% penicillin–streptomycin (Gibco), while human-derived PDX cell lines were maintained in DMEM/F12 media (Gibco) supplemented with 5% FBS (Atlas Biologicals), 1% penicillin–streptomycin (Gibco), and 1% B27 (Gibco).

#### **Nanoparticle uptake by murine and human OS cells in 2D**

For cellular uptake studies, murine and human OS cell lines were seeded at a density of 20,000 cells/well in 4-well confocal chamber slides (Thermo Fisher). Following overnight

incubation, the cells were washed with PBS and treated with rhodamine-labeled Lipo and Leuko NPs at  $3 \times 10^{11}$  particles/ml and incubated for 3, 6, and 24 h. Immediately after treatment, the supernatant was removed, cells were washed with PBS, fixed with 4% paraformaldehyde (PFA) for 10 min, and washed twice with Hank's Balanced Salt Solution (HBSS). Next, cells were stained first with 5  $\mu\text{g/ml}$  wheat germ agglutinin (WGA) S-10 Alexa Fluor™ 488 Conjugate (Invitrogen) for 10 min at 37 °C, washed twice in HBSS, and then stained with 1  $\mu\text{g/ml}$  DAPI (Abcam) for 3 min at room temperature. Imaging was acquired with Keyence BZ-X800 All-in-one Fluorescence Microscope. The images were processed using Fiji Is Just ImageJ (FIJI, version 1.53c) software.

#### **Nanoparticle uptake by murine and human OS spheroids**

Murine and human-derived PDX OS cells were seeded at 1000–2000 cells/well in complete medium for 72 h to induce OS spheroid formation before treatment. OS spheroids were incubated with rhodamine-labeled NPs for 24 h at the concentration of  $5 \times 10^{11}$  particles/ml. Subsequently, ten spheroids per condition were pooled together and washed in PBS, then fixed with 4% PFA for 10 min and washed twice with HBSS. Next, cells were stained with WGA S-10 Alexa Fluor™ 488 Conjugate (Invitrogen) and DAPI (Abcam) as previously described. Spheroids suspended in  $1 \times$  PBS were placed onto a 4-well chamber slide and z-stack images (7–10  $\mu\text{m}$  slices) were acquired on a Nikon A1 Confocal Imaging System. Images were processed using the Nikon elements software.

#### **OS cell viability assays**

In 2D settings, murine and human-derived PDX OS cell lines were seeded in a 96-well tissue culture plate at 70% confluency for overnight attachment. Cells were treated with increased concentrations of ponatinib, empty NPs (Lipo and Leuko), and Pon-loaded NPs (Lipo Pon and Leuko Pon) and cell viability was evaluated after 72 h using a MTT (3-[4,5-dimethylthiazol-2-yl]-2,5-diphenyltetrazolium bromide)-based assay (Sigma-Aldrich) according to the manufacturer's instructions. Cell viability (%) was calculated using the formula:  $(A \text{ sample}) / (A \text{ control}) \times 100$ . IC50 values for free Pon and Pon-loaded NPs (summarized in Table 2) were determined using GraphPad. Based on the Pon IC50 value determined in the 2D cell viability experiments, a range of drug dosages was selected for the 3D cell viability test. In 3D settings, OS spheroids were treated Pon, Lipo, Leuko, Lipo Pon, and Leuko Pon at concentrations equal to the Pon IC50 and  $2 \times$  IC50 values for 72 h, and viability was assessed using CellTiter-Glo® 3D Cell Viability Assay (Promega) according to the manufacturer's instructions. The optical density of each well was measured using a Spark® multimode microplate reader (Tecan).

#### **In vivo targeting and biodistribution experiments**

In vivo targeting and biodistribution experiments were performed according to the guidelines of the Animal Welfare Act, the NIH Guide for the Care and Use of Laboratory Animals, and a protocol approved by The Houston Methodist Institutional Animal Care and Use Committee (IACUC; protocol IS00006416). An orthotopic OS tumor model was generated by injecting F420 OS cells ( $1 \times 10^6$ ) into the tibia of C57Black/6 mice (6–8 weeks old). Equal populations of male and female mice were used due to the equal incidence of OS in both genders. Tumor size was measured using a caliper and volume was

calculated according to the formula:  $\text{Volume} = (a \times b^2)/2$ , where  $a$  and  $b$  represent the length and width of the tumor, respectively. When tumor volume reached  $\sim 100 \text{ mm}^3$ , Cy7-labeled NPs (100  $\mu\text{l}$ ) were administrated via tail vein injection, and mice were killed at 1, 6, and 24 h after NP injection. Fluorescent imaging (excitation/emission wavelengths: 710/760 nm) was performed using the In Vivo Imaging System (IVIS) Lumina II (PerkinElmer, Massachusetts, United States) to assess NP biodistribution in the major organs (liver, lung, spleen, kidney, and heart) and targeting in the tumors. Quantification of IVIS images was obtained by drawing regions of interest to measure average radiance (expressed as photons/s/cm<sup>2</sup>/sr) using Living Image<sup>®</sup> 4.2 software (Caliper Life Sciences, Hopkinton, MA).

#### **Intravital confocal microscopy**

Intravital microscopy (IVM) experiments were performed according to the guidelines of the Animal Welfare Act, the NIH Guide for the Care and Use of Laboratory Animals, and protocols approved by The Houston Methodist IACUC. The IVM system of the Microscopy Core at the Houston Methodist Research is an upright Nikon A1R laser scanning confocal microscope equipped with a resonance scanner, motorized and heated stage, and Nikon long-working distance 4 $\times$  and 20 $\times$  dry plan-apochromat objectives. When tumor volume reached  $\sim 100 \text{ mm}^3$ , mice were anesthetized with isoflurane and the tumor was exposed before imaging by making an incision and removing skin using a skin flap. The animal was then placed on the heated stage under the microscope and a coverslip mounted on the exposed tissue. Each of the animals was injected with 50  $\mu\text{l}$  of 0.1 mg/ml FITC-dextran to visualize the vessels and 100  $\mu\text{l}$  of Cy5.5-labeled NPs. The imaging lasted up to an hour after injection and animals were killed immediately after the imaging. All settings, including laser power, gain, offset, and pinhole diameter were maintained throughout each acquisition. All images were analyzed with NIS-Elements software. The area covered by the particles was quantified defining an intensity threshold value common to all the images. The accumulation rate was quantified by fitting with a linear regression the area change measured overtime during the first 60 min after NPs injection. Data were obtained by averaging results on at least three images from three mice.

#### **In vivo efficacy study**

In vivo efficacy experiments and animal care procedures were approved by the BCM IACUC (protocol AN-5225). Animals received humane care as per the Animal Welfare Act and the NIH Guide for the Care and Use of Laboratory Animals. An orthotopic OS tumor model was generated as previously described. Equal populations of male and female mice were used due to the equal incidence of OS in both genders. When tumor volume reached  $\sim 100 \text{ mm}^3$ , the mice were divided into groups: control groups (untreated or treated with empty Lipo or Leuko NPs) and treatment groups (free Pon or Pon-loaded Lipo or Leuko NPs). Twice a week, mice were injected IP with 30 mg/kg Pon or IV with 200  $\mu\text{l}$  of NPs for 3 weeks. All animals were euthanized the week after the last treatment or when tumor size was reaching the endpoint (1000  $\text{mm}^3$ ).

### Histological sample preparation and imaging

Mouse tissue samples from the lung, spleen, liver, kidney, and heart were washed using 1× PBS and then fixed using 10% neutral buffered formalin and embedded in paraffin. Samples were sectioned at a thickness of 4 μm and hematoxylin and eosin (H&E) staining was performed for a general pathologic inspection. The slides were imaged using the Keyence BZ-X810 microscope.

### Statistical analysis

All results were obtained from at least three independent experiments and expressed as the mean ± SD. For comparison between two groups, unpaired, two-tailed Student's *t* tests were used. Analysis of variance (ANOVA) followed by a post hoc test for multiple comparisons (Dunnett's) was used for comparison of groups of 3 or more. For Kaplan–Meier survival analysis, log-rank (Mantel–Cox) test was used. Results were considered statistically significant at *p*-values < 0.05. The statistical analysis was processed with GraphPad Prism 6 Software (GraphPad; San Diego, CA, USA).

### Abbreviations

OS	Osteosarcoma
mOS	Murine osteosarcoma
hOS	Human osteosarcoma
TKI	Tyrosine kinase inhibitor
Pon	Ponatinib
Leuko	Leukosome
Lipo	Liposome
DDS	Drug delivery system
NP	Nanoparticle
DLS	Dynamic light scattering
PDI	Polydispersity index
ZP	Zeta potential
HPLC	High-performance liquid chromatography
PDX	Patient-derived xenograft
IP	Intraperitoneal
IV	Intravenous
IVIS	In vivo imaging system
IVM	Intravital microscopy

### Supplementary Information

The online version contains supplementary material available at <https://doi.org/10.1186/s12645-022-00146-7>.

**Additional file 1: Figure S1.** High throughput screen analyses in human OS cell lines. **Figure S2.** NP physicochemical characterization. **Figure S3.** 14-day NP storage stability study. **Figure S4.** Empty biomimetic NP cytotoxicity on murine and human PDX-derived OS cell lines. **Figure S5.** Ponatinib cytotoxicity in murine and human PDX-derived OS cell lines. **Figure S6.** 2D biomimetic NP uptake on murine OS cell lines. **Figure S7.** 2D biomimetic NP uptake on human PDX-derived OS cell lines. **Figure S8.** Biomimetic NP penetration in murine OS spheroids. **Figure S9.** Biomimetic NP penetration in human PDX-derived OS spheroids. **Figure S10.** Ponatinib toxicity in murine OS spheroids. **Figure S11.** Ponatinib toxicity in human PDX-derived OS spheroids. **Figure S12.** Biomimetic NPs in vivo tumor targeting. **Figure S13.** Empty NPs toxicity. **Figure S14.** In vivo efficacy study.

### Acknowledgements

The authors would like to thank Amanda Weiskoff (Academic Affairs, Houston Methodist Academic Institute) for scientific editing assistance and Assaf Zinger for the optimization and supervision of the nanoparticle formulation. The authors would like to thank the Neal Cancer Center cores of HMRI for their invaluable contributions.

### Author contributions

FG and SL designed and performed the experiments, executed the data collection and analyses, wrote the manuscript and prepared the figures. GB and AE performed synthesis of nanoparticles. RR and MM assisted in the 2D in vitro experiments for the NPs uptake, toxicity assay and reviewed the manuscript. EDR performed the IVM experiments and analyses.

LK assisted in vivo experiments. MA reviewed the manuscript. FT and JTY provided supervision and intellectual input throughout the project, and reviewed the manuscript. All authors read and approved the final manuscript.

#### Funding

Research reported in this publication was supported by the Cancer Prevention and Research Institute of Texas (CPRI-TRP180394) to FT and JTY.

#### Availability of data and materials

All data and materials will be available under direct request.

#### Declarations

##### Ethics approval and consent to participate

All animal studies were performed in accordance with the guidelines of the Animal Welfare Act and the Guide for the Care and Use of Laboratory Animals, following protocols approved by the Institutional Animal Care and Use Committee (IACUC, protocol IS00006416) at the Houston Methodist Research Institute.

##### Consent for publication

All authors have agreed to publish this manuscript.

##### Competing interests

The authors declare that this manuscript is original, has not been published before and is not currently being considered for publication elsewhere. The authors declare no conflict of interest.

Received: 20 July 2022 Accepted: 10 October 2022

Published online: 02 December 2022

#### References

- Abu-Hijleh MF, Habbal OA, Moqattash ST (1995) The role of the diaphragm in lymphatic absorption from the peritoneal cavity. *J Anat* 186(Pt 3):453
- Al Shihabi A, Davarifar A, Nguyen HTL, Tavanaie N, Nelson SD, Yanagawa J et al (2021) Personalized chordoma organoids for drug discovery studies. *bioRxiv*. <https://doi.org/10.1126/sciadv.abc3674>
- Al Shoyaib A, Archie SR, Karamyan VT (2020) Intraperitoneal route of drug administration: should it be used in experimental animal studies? *Pharm Res* 37(1):1–17
- Anselmo AC, Mitragotri S (2019) Nanoparticles in the clinic: an update. *Bioeng Transl Med* 4(3):e10143
- Boada C, Zinger A, Tsao C, Zhao P, Martinez JO, Hartman K et al (2020) Rapamycin-loaded biomimetic nanoparticles reverse vascular inflammation. *Circul Res* 126(1):25–37
- Buddingh EP, Kuijjer ML, Duim RA, Bürger H, Agelopoulos K, Myklebost O et al (2011) Tumor-infiltrating macrophages are associated with metastasis suppression in high-grade osteosarcoma: a rationale for treatment with macrophage activating agents. *Clin Cancer Res* 17(8):2110–2119
- Chang T, Olson J, Proffitt R, Adler-Moore J (2010) Differences in tissue drug concentrations following intravenous versus intraperitoneal treatment with amphotericin B deoxycholate or liposomal amphotericin B. *Med Mycol* 48(2):430–435
- Chen J, Ning E, Wang Z, Jing Z, Wei G, Wang X et al (2021) Docetaxel loaded mPEG-PLA nanoparticles for sarcoma therapy: preparation, characterization, pharmacokinetics, and anti-tumor efficacy. *Drug Deliv* 28(1):1389–1396
- Cheng Z, Li M, Dey R, Chen Y (2021) Nanomaterials for cancer therapy: current progress and perspectives. *J Hematol Oncol* 14(1):1–27
- Chu KS, Schorzman AN, Finnis MC, Bowerman CJ, Peng L, Luft JC et al (2013) Nanoparticle drug loading as a design parameter to improve docetaxel pharmacokinetics and efficacy. *Biomaterials* 34(33):8424–8429
- Corbo C, Molinaro R, Taraballi F, Toledano Furman NE, Hartman KA, Sherman MB et al (2017a) Unveiling the in vivo protein corona of circulating leukocyte-like carriers. *ACS Nano* 11(3):3262–3273
- Corbo C, Cromer WE, Molinaro R, Furman NET, Hartman KA, De Rosa E et al (2017b) Engineered biomimetic nanovesicles show intrinsic anti-inflammatory properties for the treatment of inflammatory bowel diseases. *Nanoscale* 9(38):14581–14591
- Cortes JE, Talpaz M, Kantarjian H (2014) Ponatinib in Philadelphia chromosome-positive leukemias. *N Engl J Med* 370(6):577
- De Lin RK, Huang JT-J, Henderson CJ, Wolf CR (2017) Novel pathways of ponatinib disposition catalyzed by CYP1A1 involving generation of potentially toxic metabolites. *J Pharmacol Exp Ther* 363(1):12
- Eilber F, Giuliano A, Eckardt J, Patterson K, Moseley S, Goodnight J (1987) Adjuvant chemotherapy for osteosarcoma: a randomized prospective trial. *J Clin Oncol* 5(1):21–26
- Evola FR, Costarella L, Pavone V, Caff G, Cannavò L, Sessa A et al (2017) Biomarkers of osteosarcoma, chondrosarcoma, and ewing sarcoma. *Front Pharmacol* 8:150
- Fernandes C, Soares D, Yergeri MC (2018) Tumor microenvironment targeted nanotherapy. *Front Pharmacol* 9:1230
- Gainor JF, Chabner BA (2015) Ponatinib: accelerated disapproval. *Oncologist* 20(8):847
- Gao Y, Shen JK, Choy E, Zhang Z, Mankin HJ, Hornicek FJ et al (2016) Pharmacokinetics and tolerability of NSC23925b, a novel P-glycoprotein inhibitor: preclinical study in mice and rats. *Sci Rep* 6(1):1–10
- Gao Z, Zhao GS, Lv Y, Peng D, Tang X, Song H et al (2019) Anoikis-resistant human osteosarcoma cells display significant angiogenesis by activating the src kinase-mediated MAPK pathway. *Oncol Rep* 41(1):235–245
- Gill J, Gorlick R (2021) Advancing therapy for osteosarcoma. *Nat Rev Clin Oncol* 18:1–16

- Giordano F, Lenna S, Rampado R, Brozovich A, Hirase T, Tognon MG et al (2021) Nanodelivery systems face challenges and limitations in bone diseases management. *Adv Ther* 4:2100152
- Guan X, Guan Z, Song C (2020) Expression profile analysis identifies key genes as prognostic markers for metastasis of osteosarcoma. *Cancer Cell Int* 20(1):1–10
- Guichard S, Chatelut E, Lochon I, Bugat R, Mahjoubi M, Canal P (1998) Comparison of the pharmacokinetics and efficacy of irinotecan after administration by the intravenous versus intraperitoneal route in mice. *Cancer Chemother Pharmacol* 42(2):165–170
- Han SJ, Kwon S, Kim KS (2021) Challenges of applying multicellular tumor spheroids in preclinical phase. *Cancer Cell Int* 21(1):1–19
- Harrison DJ, Geller DS, Gill JD, Lewis VO, Gorlick R (2018) Current and future therapeutic approaches for osteosarcoma. *Expert Rev Anticancer Ther* 18(1):39–50
- Hattinger CM, Patrizio MP, Fantoni L, Casotti C, Riganti C, Serra M (2021) Drug resistance in osteosarcoma: emerging biomarkers, therapeutic targets and treatment strategies. *Cancers* 13(12):2878
- Hoy SM (2014) Ponatinib: a review of its use in adults with chronic myeloid leukaemia or Philadelphia chromosome-positive acute lymphoblastic leukaemia. *Drugs* 74(7):793–806
- Hu C, Deng Z, Zhang Y, Yan L, Cai L, Lei J et al (2015) The prognostic significance of src and p-Src expression in patients with osteosarcoma. *Med Sci Monit Int Med J Exp Clin Res* 21:638
- Huang L, Jiang S, Shi Y (2020) Tyrosine kinase inhibitors for solid tumors in the past 20 years (2001–2020). *J Hematol Oncol* 13(1):1–23
- Janeway KA, Grier HE (2010) Sequelae of osteosarcoma medical therapy: a review of rare acute toxicities and late effects. *Lancet Oncol* 11(7):670–678
- Jiao Q, Bi L, Ren Y, Song S, Wang Q, Wang YS (2018) Advances in studies of tyrosine kinase inhibitors and their acquired resistance. *Mol Cancer* 17(1):1–12
- Joyce JA, Pollard JW (2009) Microenvironmental regulation of metastasis. *Nat Rev Cancer* 9(4):239–252
- Kovshova T, Osipova N, Alekseeva A, Malinovskaya J, Belov A, Budko A et al (2021) Exploring the interplay between drug release and targeting of lipid-like polymer nanoparticles loaded with doxorubicin. *Molecules* 26(4):831
- Lee YT, Tan YJ, Oon CE (2018) Molecular targeted therapy: treating cancer with specificity. *Eur J Pharmacol* 834:188–196
- Liu B, Huang Y, Sun Y, Zhang J, Yao Y, Shen Z et al (2016) Prognostic value of inflammation-based scores in patients with osteosarcoma. *Sci Rep* 6(1):1–9
- Liu Y, Li Q, Bai Q, Jiang W (2021) Advances of smart nano-drug delivery systems in osteosarcoma treatment. *J Mater Chem B* 9(27):5439–5450
- Lukas G, Brindle SD, Greengard P (1971) The route of absorption of intraperitoneally administered compounds. *J Pharmacol Exp Ther* 178(3):562–566
- Martinez JO, Molinaro R, Hartman KA, Boada C, Sukhovshin R, De Rosa E et al (2018) Biomimetic nanoparticles with enhanced affinity towards activated endothelium as versatile tools for theranostic drug delivery. *Theranostics* 8(4):1131
- Massaro F, Molica M, Breccia M (2018) Ponatinib: a review of efficacy and safety. *Curr Cancer Drug Targets* 18(9):847–856
- Misaghi A, Goldin A, Awad M, Kulidjian AA (2018) Osteosarcoma: a comprehensive review. *SICOT-J* 4:12
- Molica M, Scalzulli E, Colafigli G, Foà R, Breccia M (2019) Insights into the optimal use of ponatinib in patients with chronic phase chronic myeloid leukaemia. *Ther Adv Hematol* 10:2040620719826444
- Molinaro R, Corbo C, Martinez JO, Taraballi F, Evangelopoulos M, Minardi S et al (2016a) Biomimetic proteolipid vesicles for targeting inflamed tissues. *Nat Mater* 15(9):1037–1046
- Molinaro R, Boada C, Del Rosal GM, Hartman KA, Corbo C, Andrews ED et al (2016b) Vascular inflammation: a novel access route for nanomedicine. *Methodist Debakey Cardiovasc J* 12(3):169
- Molinaro R, Evangelopoulos M, Hoffman JR, Corbo C, Taraballi F, Martinez JO et al (2018) Design and development of biomimetic nanovesicles using a microfluidic approach. *Adv Mater* 30(15):1702749
- Molinaro R, Pasto A, Corbo C, Taraballi F, Giordano F, Martinez JO et al (2019) Macrophage-derived nanovesicles exert intrinsic anti-inflammatory properties and prolong survival in sepsis through a direct interaction with macrophages. *Nanoscale* 11(28):13576–13586
- Molinaro R, Pasto A, Taraballi F, Giordano F, Azzi JA, Tasciotti E et al (2020a) Biomimetic nanoparticles potentiate the anti-inflammatory properties of dexamethasone and reduce the cytokine storm syndrome: an additional weapon against COVID-19? *Nanomaterials* 10(11):2301
- Molinaro R, Martinez JO, Zinger A, De Vita A, Storci G, Arrighetti N et al (2020b) Leukocyte-mimicking nanovesicles for effective doxorubicin delivery to treat breast cancer and melanoma. *Biomater Sci* 8(1):333–341
- Musumeci F, Greco C, Grossi G, Molinari A, Schenone S (2018) Recent studies on ponatinib in cancers other than chronic myeloid leukemia. *Cancers* 10(11):430
- Nakano K, Takahashi S (2018) Current molecular targeted therapies for bone and soft tissue sarcomas. *Int J Mol Sci* 19(3):739
- Pasto A, Giordano F, Evangelopoulos M, Amadori A, Tasciotti E (2019) Cell membrane protein functionalization of nanoparticles as a new tumor-targeting strategy. *Clin Transl Med* 8(1):1–9
- Petschauer JS, Madden AJ, Kirschbrown WP, Song G, Zamboni WC (2015) The effects of nanoparticle drug loading on the pharmacokinetics of anticancer agents. *Nanomedicine* 10(3):447–463
- Picci P, Ferrari S, Bacci G, Gherlinzoni F (1994) Treatment recommendations for osteosarcoma and adult soft tissue sarcomas. *Drugs* 47(1):82–92
- Rathore R, Van Tine BA (2021) Pathogenesis and current treatment of osteosarcoma: perspectives for future therapies. *J Clin Med* 10(6):1182
- Rothenaigier I, Hadian K (2021) Brief guide: experimental strategies for high-quality hit selection from small-molecule screening campaigns. *SLAS Discov Adv Sci Drug Discov* 26(7):851–854
- Russo E, Spallarossa A, Tasso B, Villa C, Brullo C (2021) Nanotechnology of tyrosine kinase inhibitors in cancer therapy: a perspective. *Int J Mol Sci* 22(12):6538

- Sevela F, Mayr L, Kubista B, Lötsch D, van Schoonhoven S, Windhager R et al (2015) EGFR is not a major driver for osteosarcoma cell growth in vitro but contributes to starvation and chemotherapy resistance. *J Exp Clin Cancer Res* 34(1):1–12
- Shimada T, Nomura M, Yokogawa K, Endo Y, Sasaki T, Miyamoto KI et al (2005) Pharmacokinetic advantage of intraperitoneal injection of docetaxel in the treatment for peritoneal dissemination of cancer in mice. *J Pharm Pharmacol* 57(2):177–181
- Smidova V, Michalek P, Goliasova Z, Eckschlagler T, Hodek P, Adam V et al (2021) Nanomedicine of tyrosine kinase inhibitors. *Theranostics* 11(4):1546
- Sushnitha M, Evangelopoulos M, Tasciotti E, Taraballi F (2020) Cell membrane-based biomimetic nanoparticles and the immune system: immunomodulatory interactions to therapeutic applications. *Front Bioeng Biotechnol* 8:627
- Tan FH, Putoczki TL, Stylli SS, Luwor RB (2019) Ponatinib: a novel multi-tyrosine kinase inhibitor against human malignancies. *Oncotargets and therapy* 12:635
- Tchoryk A, Taresco V, Argent RH, Ashford M, Gellert PR, Stolnik S et al (2019) Penetration and uptake of nanoparticles in 3D tumor spheroids. *Bioconjug Chem* 30(5):1371–1384
- Tian Z, Niu X, Yao W (2020) Receptor tyrosine kinases in osteosarcoma treatment: which is the key target? *Front Oncol* 10:1642
- Urciuoli E, Coletta I, Rizzuto E, De Vito R, Petrini S, D’Oria V et al (2018) Src nuclear localization and its prognostic relevance in human osteosarcoma. *J Cell Physiol* 233(2):1658–1670
- US FDA (2013) FDA Drug Safety Communication: FDA asks manufacturer of the leukemia drug Iclusig (ponatinib) to suspend marketing and sales. US FDA, Silver Spring
- Van Zundert I, Fortuni B, Rocha S (2020) From 2D to 3D cancer cell models—the enigmas of drug delivery research. *Nanomaterials* 10(11):2236
- Wang D, Niu X, Wang Z, Song C-L, Huang Z, Chen K-N et al (2019) Multiregion sequencing reveals the genetic heterogeneity and evolutionary history of osteosarcoma and matched pulmonary metastases. *Cancer Res* 79(1):7–20
- Wang S-Y, Hu H-Z, Qing X-C, Zhang Z-C, Shao Z-W (2020) Recent advances of drug delivery nanocarriers in osteosarcoma treatment. *J Cancer* 11(1):69
- Whelan J, Bielack S, Marina N, Smeland S, Jovic G, Hook J et al (2015) EURAMOS-1, an international randomised study for osteosarcoma: results from pre-randomisation treatment. *Ann Oncol* 26(2):407–414
- Wilding CP, Elms ML, Judson I, Tan A-C, Jones RL, Huang PH (2019) The landscape of tyrosine kinase inhibitors in sarcomas: looking beyond pazopanib. *Expert Rev Anticancer Ther* 19(11):971–991
- Wood GE, Hockings H, Hilton DM, Kermorgant S (2021) The role of MET in chemotherapy resistance. *Oncogene* 40(11):1927–1941
- Xu X, Farach-Carson MC, Jia X (2014) Three-dimensional in vitro tumor models for cancer research and drug evaluation. *Biotechnol Adv* 32(7):1256–1268
- Xu J, Xie L, Guo W (2018) PDGF/PDGFR effects in osteosarcoma and the “add-on” strategy. *Clin Sarcoma Res* 8(1):1–9
- Yao S, Li L, Su X-T, Wang K, Lu Z-J, Yuan C-Z et al (2018) Development and evaluation of novel tumor-targeting paclitaxel-loaded nano-carriers for ovarian cancer treatment: in vitro and in vivo. *J Exp Clin Cancer Res* 37(1):1–13
- Zamborsky R, Kokavec M, Harsanyi S, Danisovic L (2019) Identification of prognostic and predictive osteosarcoma biomarkers. *Med Sci* 7(2):28
- Zhang M, Du Y, Wang S, Chen B (2020) A review of biomimetic nanoparticle drug delivery systems based on cell membranes. *Drug Des Dev Ther* 14:5495
- Zhao X, Wu Q, Gong X, Liu J, Ma Y (2021) Osteosarcoma: a review of current and future therapeutic approaches. *Biomed Eng Online* 20(1):1–14
- Zhou X, Shi K, Hao Y, Yang C, Zha R, Yi C et al (2020) Advances in nanotechnology-based delivery systems for EGFR tyrosine kinases inhibitors in cancer therapy. *Asian J Pharm Sci* 15(1):26–41
- Zinger A, Baudo G, Naoi T, Giordano F, Lenna S, Massaro M et al (2020) Reproducible and characterized method for ponatinib encapsulation into biomimetic lipid nanoparticles as a platform for multi-tyrosine kinase-targeted therapy. *ACS Appl Bio Mater* 3(10):6737–6745
- Zinger A, Sushnitha M, Naoi T, Baudo G, De Rosa E, Chang J et al (2021) Enhancing inflammation targeting using tunable leukocyte-based biomimetic nanoparticles. *ACS Nano* 15(4):6326–6339

## Publisher's Note

Springer Nature remains neutral with regard to jurisdictional claims in published maps and institutional affiliations.

Ready to submit your research? Choose BMC and benefit from:

- fast, convenient online submission
- thorough peer review by experienced researchers in your field
- rapid publication on acceptance
- support for research data, including large and complex data types
- gold Open Access which fosters wider collaboration and increased citations
- maximum visibility for your research: over 100M website views per year

At BMC, research is always in progress.

Learn more [biomedcentral.com/submissions](https://biomedcentral.com/submissions)

